



# Total Control

*Advanced integrated supervisory and wind turbine control for optimal operation of large Wind Power Plants*

*Title: Simple dynamic wind farm model*  
*Deliverable no.: D1.9*

*Delivery date: (31.03.2019)*  
*Lead beneficiary: DNV*  
*Dissemination level: Public*



*This project has received funding from the European Union's Horizon 2020 Research and Innovation Programme under grant agreement No. 727680*

**Author(s) information (alphabetical):**

Name	Organisation	Email
Ervin Bossanyi	DNV GL	ervin.bossanyi@dnvgl.com
Renzo Ruisi	DNV GL	renzo.ruisi@dnvgl.com

**Acknowledgements/Contributions:**

Name	Name	Name
Gunner Larsen	Ingemar Carlen	Peder Enevoldsen
For their help with wind farm SCADA data, turbine characteristics and meteorological information from Lillgrund wind farm		

**Document information**

Version	Date	Description			
1	15.03.2019	Draft	Prepared by Ervin Bossanyi	Reviewed by Johan Meyers	Approved by Ervin Bossanyi
2	29.03.2019	Final	Ervin Bossanyi	Johan Meyers	Ervin Bossanyi

**Definitions**


# 1 TABLE OF CONTENTS

Executive summary .....	5
Introduction .....	6
2 Model description .....	7
2.1 Model purpose and specification .....	7
2.2 Turbine aerodynamics.....	7
2.3 Turbine dynamics .....	7
2.4 Turbine control – power production.....	8
2.5 Turbine control – supervisory .....	8
2.6 Turbine loads .....	8
2.7 Wind field .....	9
2.7.1 Wind shear.....	10
2.8 Wake model.....	10
2.8.1 Wake deficit profile .....	10
2.8.2 Wake turbulence .....	12
2.8.3 Wake deflection .....	12
2.8.4 Wake superposition .....	12
2.8.5 Wake meandering.....	13
2.8.6 Wake advection.....	14
2.9 Wind farm control.....	14
2.10 <i>LongSim</i> usage .....	15
3 Validation data .....	16
3.1 Turbine information.....	16
3.1.1 Turbine model .....	16
3.1.2 Effect of yaw misalignment .....	17
3.2 SCADA data.....	18
3.3 Meteorological data .....	18
3.3.1 Meteorological data from the Drogden Lighthouse.....	19
3.3.2 Characterisation of the atmospheric stability at the site .....	19
4 Wake model validation .....	23
4.1 Wake modelling and atmospheric stability.....	23
4.1.1 Inputs and wake models used .....	23
4.1.2 Results from Steady-state wake modelling at the Lillgrund offshore site.....	25

5	Dynamic simulation .....	31
5.1	Introduction.....	31
5.2	Wind field generation .....	31
5.3	Initial results .....	32
5.4	Further simulation results.....	41
5.5	Conclusions from the dynamic simulation results .....	47
6	Application to wind farm control .....	48
6.1	Introduction.....	48
6.1.1	Wake steering – setpoint optimisation.....	48
6.1.2	Wake steering – testing in dynamic simulation .....	50
7	Conclusions .....	53
7.1	Wake modelling.....	53
7.2	Dynamic simulation.....	53
7.3	Wind farm control.....	54
	References .....	54

## EXECUTIVE SUMMARY

DNV GL's wind farm simulation code *LongSim* is an engineering code designed to simulate the dynamic behaviour of turbines and their wakes within a realistic wind field. It includes various engineering simplifications, especially in terms of the flow modelling and wind turbine aeroelastic behaviour, so as to achieve sufficient calculation speed to allow repeated control design iterations and long simulations to be carried out easily, with minimal computing power.

This report presents the results of a model validation exercise, in which the performance of the simulation model is compared against SCADA data from Lillgrund offshore wind farm near Copenhagen.

Firstly, mean power ratio methods are used to compare different wake models which are available in *Longsim* against 5-minute average SCADA data. A study on the atmospheric stability conditions at the site is performed based on nonconcurrent data from the nearby Drogden lighthouse, from which a potential link between strong unstable conditions and time-of-day is found. Comparisons are then performed both for narrow wind direction bins ( $300^{\circ}\pm 2.5^{\circ}$ ) and larger wind direction bins ( $300^{\circ}\pm 15^{\circ}$ ), and with different filtering strategies. A wake model which was tuned for unstable atmospheric conditions is found to perform better in terms of power predictions, even though a neutral-based standard model is found to perform reasonably well when compared to power production filtered for narrow directional bins. It is noted that the small inter-turbine spacing and the uncertainties on the non-calibrated SCADA data will affect the predictions.

Secondly, dynamic simulations are run using *LongSim*, driven by stochastic wind fields generated from wind conditions derived from the SCADA data itself. The simulation results are compared in detail to the SCADA data for each turbine. During this exercise, significant issues were identified with the raw SCADA data which make it difficult to compare results very closely, or to validate some of the finer points of the model. Nevertheless, the results appear to be very plausible, indicating that the model is a suitable and appropriate tool for investigation of wind farm control possibilities.

Finally, an example of the use of the model for wind farm control design is presented. A wake steering controller is designed, using *Longsim*'s steady-state setpoint optimisation capability, and tested by running a dynamic simulation using a stochastic wind field generated using site wind conditions. Preliminary results show that a significant increase in energy production can be obtained, although further simulations aimed at reducing the yaw actuator duty would be desirable. The results indicate the importance of doing such dynamic simulations as part of the design process. *LongSim* can also be used in the same way for induction controller design, where power setpoints are modified to optimise total wind farm performance.

## INTRODUCTION

This report concerns DNV GL's wind farm simulation model *LongSim*. By validating the model against measured data from the Lillgrund offshore wind farm, the aim is to demonstrate the usefulness of the model for design and testing of wind farm controllers.

This model was developed originally by DNV GL starting in 2012 to help tune supervisory control parameters of a single wind turbine in the context of site-specific long-term wind conditions, as reported in [1]. To capture the important turbine control dynamics it runs with a timestep of around one second, and yet it can run very long simulations (several years if necessary), driven by site-specific met mast data, in order to capture the statistics of relatively infrequent supervisory control events which depend on low-frequency variations in meteorological conditions.

This combination of short timesteps and long simulation times is ideal for designing wind farm controllers, and testing them over realistically changing wind conditions. DNV GL has therefore extended this model to cover a whole wind farm, by generating a correlated wind field over the whole farm, adding a dynamic model for wake effects, extending the turbine controllers to respond to wind farm controller demands, and adding a wind farm controller to generate these demands.

In order to achieve the rapid calculation times required for iterative optimisation of wind farm control setpoints as well as for long simulations over changing conditions, an engineering approach to the wind farm flow modelling has been adopted, as any sort of complete Computation Fluid Dynamic (CFD) solution of the Navier Stokes equations would be prohibitive in computer time. The approach makes use of an ambient flow field created from measured data (such as from a meteorological mast, for instance) enhanced with synthetic turbulence generated to be consistent with known or assumed statistical properties (defined in terms of wavenumber spectrum and coherence), into which the wakes are subsequently embedded. This allows only one-way interaction from the ambient flow field to the wakes, although some modification of the ambient flow through 'large wind farm effects' can be included. Different engineering wake models are available in *LongSim*, the main ones being based on simplified CFD solutions.

An illustration of the use of the model for testing wind farm controllers is reported in [2] and [3]. The model has also been used for wind farm controller design and testing during the Horizon 20-20 project CL-Windcon [4], as well as in commercial projects.

The model is described in more detail in Section 2.

In the TotalControl project, the availability of a detailed dataset from Lillgrund wind farm presents the opportunity to perform a model validation exercise with the aim of confirming the ability of the model to predict the relevant aspects of a wind farm's behaviour, and hence to increase confidence in its usefulness as a tool for wind farm controller design and testing. Section 2.8.2 describes the validation data available from Lillgrund which has been used so far for this exercise.

The validation has been done in two stages: validation of the engineering wake models themselves, followed by validation of the overall dynamic performance of the wind farm. Section 4 describes the wake model validation exercise, allowing a validated wake model to be used for validation of the dynamic wind farm performance in Section 5. Finally, Section 6 presents a simple preliminary illustration showing how the model might be used to design and test a wind farm controller for Lillgrund wind farm.

## 2 MODEL DESCRIPTION

### 2.1 MODEL PURPOSE AND SPECIFICATION

The *LongSim* model has been developed internally by DNV GL, for the purpose of exploring the possibilities of wind farm control, and testing and evaluating wind farm control algorithms in a realistic dynamic environment. The model is designed for low computational cost so that different control options can be investigated rapidly. Although starting with relatively low-fidelity empirical models, the intention is to allow more sophisticated models to be implemented easily when this becomes appropriate. This table gives an outline specification:

Computational cost	To run in real time on a typical laptop for a wind farm of ~100 turbines
Turbine aerodynamics	Either power and thrust curves, or $C_p$ & $C_T$ as functions of tip speed ratio, pitch angle, yaw misalignment
Turbine dynamics	Rotor speed, pitch & yaw DOFs are available
Turbine control	Generator torque, blade pitch, and yaw control
Turbine loads	Database look-up from previous high-fidelity <i>Bladed</i> simulations
Timestep	~ 1 second
Input wind data	Met mast 10-minute averages (typically) or similar
Simulation length	Hours to years
Wind field	Low frequencies correlated across farm, evolving as it advects
Wake profile	Ainslie model initially, other models available
Wake turbulence	Quarton-Ainslie model initially, other models available
Wake meandering	Driven by low-frequency turbulence in wind field
Wake advection	Driven by low-frequency wind field with wake deficit modification
Wake deflection	Jímenez model initially, other models available
Wind farm control	Power delta and/or yaw offset, coordinated yaw control, etc.

### 2.2 TURBINE AERODYNAMICS

The aerodynamic power and thrust of the whole rotor are modelled (without resolving individual blades). These are defined by look-up tables, either as steady power and thrust curves as a function of wind speed, or as power and thrust coefficients as a function of tip speed ratio and pitch angle. For many applications, the changes in power and thrust with yaw misalignment should also be specified. The effect of yaw misalignment may be important, firstly to be able to predict power production accurately given the inevitable yaw misalignment variations which occur in practice and in the model, and secondly to be able to model any deliberate yaw misalignments due to wake steering control.

The effect of yaw can be modelled in various ways: either a series of look-up tables can be supplied for different yaw angles, or empirical correction formulae can be applied to the power and thrust. These corrections are typically obtained by running a set of simulations with DNV GL's aeroelastic code *Bladed*, using steady wind conditions for different yaw misalignments.

The modelling assumptions used in this report are detailed in Section 3.1.

### 2.3 TURBINE DYNAMICS

A simple dynamic model is used, consistent with using a timestep in the region of 1 second, so higher-frequency structural dynamics are not represented. The rotor speed and blade pitch degrees of freedom can be activated if desired, together with nacelle yaw. The first tower fore-aft mode could be readily implemented if desired.

Sensor and actuator responses currently modelled are:

- Speed sensor time constant
- Generator torque actuation time constant
- Pitch actuation time constant and/or second-order response
- Yawing at constant rate

The rotor speed and pitch degrees of freedom are used if the rotor is represented by power and thrust coefficient tables. If only steady power and thrust curves are provided, then this is not possible.

## 2.4 TURBINE CONTROL – POWER PRODUCTION

The rotor speed and pitch degrees of freedom are used, standard PI(D)-based torque and collective pitch control are implemented, with pitch gain scheduling. Below-rated  $C_P$ -tracking uses either a standard quadratic gain or a look-up table. Transitions at rated wind speed between torque and pitch control use bias terms. All these features are defined in [5]. The bias terms are calculated from an estimated wind speed, for which a Luenberger observer is available, but an ideal estimator using the rotor-average wind speed is usually allowable given the time step used.

Delta control is implemented as described in [6], and can be used for wind farm induction control and/or as an ancillary service for the grid. The estimated wind speed drives a parallel representation of the turbine and controller dynamics without delta control (and without yaw misalignment) to define the maximum power available at any instant. The power delta is subtracted from this, and the torque demand to the power converter is reduced by the amount necessary to achieve this reduced power. At the same time, the fine pitch is increased to maintain the desired rotor speed. The net result is that the power reduction is achieved by increasing the pitch angle while keeping the same rotor speed. Other options for active power control are readily implementable if required.

If only steady power and thrust curves are available, then the torque and pitch control dynamics cannot be modelled. However, delta control can still be modelled by providing separate power and thrust curves for different delta setpoints.

## 2.5 TURBINE CONTROL – SUPERVISORY

Supervisory control (including yaw control) is flexibly implemented. A syntax is provided so that the user can define typical filters, counters, alarms, etc. Filters are typically low-pass filters for generator speed, yaw misalignment (from the wind vane signal), wind speed (from the nacelle anemometer) etc. Alarms can respond to filter and counter outputs using conditions which can include thresholds and durations (time since threshold crossing), latches, etc. Nacelle anemometry corrections for rotor influence are assumed to be included in the calibrations.

## 2.6 TURBINE LOADS

To run fast, the turbine model does not include structural dynamics nor spatial variations in turbulence across the rotor, and is cannot therefore generate fatigue loads during the simulation. Fatigue loads are therefore obtained in a post-processing step using a Fatigue Loads Database (FLD) pre-calculated for a single turbine using a detailed *Bladed* model, with full structural dynamics, turbulence, control etc. (including any wind farm control actions). Damage equivalent loads are calculated for 10-minute simulations over a range of wind speeds, turbulence

intensities, yaw misalignments, delta set-points, etc. and stored in a multi-dimensional look-up table.

This is a pragmatic approach, which ignores some effects which could have some importance. For example, wake turbulence does not have the same characteristics as ambient turbulence with just an increase in turbulence intensity; and low-frequency variations such as wake meandering will also affect the fatigue loading to some extent. Further research is aimed at quantifying any corrections for these affects which may be desirable.

## 2.7 WIND FIELD

The wind field is made up of low-frequency and high-frequency variations. These are separated in order to minimise computation requirements while maintaining the most important features of the wind field. The boundary between the low and high frequency regions is defined by a user-specified cut-off wavelength, typically corresponding to a spatial resolution of around two turbine diameters ( $\Delta x = 2D$ ). Lower-frequency variations are correlated across the wind farm, making use of coherence functions, and are also assumed to drive wake meandering. Higher-frequency variations are assumed to be uncorrelated between turbines. They affect the turbine behaviour and loads, but do not affect wake meandering.

The entire wind field is generated starting from single-point measured data from e.g. a met mast, usually consisting of 10-minute averages of wind speed, direction and standard deviation. The first step is to generate a smooth time history of wind speed and direction such that each 10-minute section has the correct (measured) mean value, and whose value and gradient are continuous at the 10-minute boundaries. This is done by selecting start and end values and gradients for each 10-minute section, and fitting a quartic function in between. Synthetic turbulence is then added to this smooth time history. In the absence of faster-sampled data, the form of the turbulence spectrum needs to be assumed, e.g. the Kaimal spectrum, but the amplitude of the turbulence is then scaled to match the measured standard deviation. The spectrum is divided into two at the cut-off wavelength corresponding to  $\Delta x$ .

The low-frequency variations must cover the entire range of wind speeds and directions in the measured dataset. For this reason, the spectrum and coherence functions are expressed in terms of wavenumber rather than frequency, as they then become largely independent of wind speed. For each 10-minute section (length  $T = 600s$ ), synthetic turbulence is added using the part of the turbulence spectrum from  $1/T$  up to the frequency corresponding to  $\Delta x$ . The entire time history is then resampled to points uniformly spaced in alongwind distance  $x$  and converted into a wavenumber spectrum using a Fast Fourier Transform (FFT). Using a suitable coherence function, the method of Veers [7] is used to generate correlated histories at a grid of points covering the wind farm area at hub height. To simulate advection, the phases of components at wavenumber  $k$  are adjusted by  $2\pi kx$  at downwind distance  $x$  prior to the inverse FFT. The histories are converted back to the time domain by resampling at the original time points.

There is some uncertainty over suitable coherence functions to use. For turbine rotors, the IEC standard [8] provides lateral and vertical coherence functions which can be used for the higher frequencies. Several of these are implemented in the model, with Kaimal as the default option. This does not specify the along-wind coherence however, so an exponential decay model is assumed for this:

$$\text{coh}(k,d) = \exp(-\beta kd) \quad (1)$$

at wavenumber  $k = f/U$  for separation  $d$ . However, there is some uncertainty over the decay parameter  $\beta$ .

The Larsen exponential model [9] for mesoscale coherence is used as the default for lower frequencies:

$$\text{coh}(k,d) = \exp[(1.8\cos(2\theta) - 5.9)kd] \quad (2)$$

for separation  $d$  at angle  $\theta$  to the flow direction. A gradual transition between the two models occurs over a user-specified range of intermediate wavenumbers.

In the alongwind direction ( $\theta = 0$ ), the Larsen model for mesoscale variations would be equivalent to  $\beta = 4.1$  in the exponential model for alongwind turbulent fluctuations. This compares to the value of  $\beta \approx 7$  for turbulent fluctuations suggested by Panofsky [10]. However, the Kristensen model [11] implies a value an order of magnitude smaller, while the LiDAR measurements of Schlipf [12] show values of  $\beta$  in the range of about 0.4 - 1.25, albeit over somewhat smaller distances than are relevant here.

The low-frequency wind field generated in this way contains variations in all three components: longitudinal, lateral and vertical. However, the lateral and vertical components are zero-mean and therefore do not account for gross changes in wind direction. This is therefore simulated by rotating the entire wind field about a notional reference point by the current direction taken from the smoothed measured direction history. However, this is unrealistic for rapid direction changes so an assumption has to be made about how the direction change propagates through the farm, namely that it propagates at the mean speed, and the local wind vectors are rotated accordingly.

The low-frequency wind field is generated in the absence of turbines and their wakes. The wake deficits described below are then superimposed on this undisturbed wind field. This means that any effects of the turbines and their wakes on the underlying flow is neglected. This includes for example, wind farm blockage effects causing general flow speed reduction, and any change in the advection of turbulence caused by reduced wake flow velocities. However, pre-calculated terrain and large wind farm effects on the ambient flow can be accommodated.

### 2.7.1 WIND SHEAR

Wind shear can be superimposed on the wind field, giving a variation of wind speed with height across the rotor. The standard logarithmic and fixed exponent models are available.

## 2.8 WAKE MODEL

A number of different models are available within the *LongSim* code to model the various relevant wake characteristics. These are all engineering models with some empirical features, and to some extent, models for the different wake characteristics can be brought together in different combinations. The models for the specific wake characteristics are described in the following subsections.

### 2.8.1 WAKE DEFICIT PROFILE

The wake profile describes how the velocity deficit varies across the wake. Beyond a short “near wake” region, the profile can be considered to spread as it moves further downstream, becoming broader and shallower (so as to obey momentum conservation) while maintaining its general shape. The rate of spreading increases with turbulence intensity.

The very simple Jensen model consists of a rectangular profile, combined with a linear spreading rate which is purely empirical. Although (by selecting the right spreading rate) it can work surprisingly well for overall energy capture results, it is considered too crude for this application. Two main models are used instead, both of which have a Gaussian-shaped profile.

The default model for the wake velocity deficit profile is the Ainslie model [13], which uses a simplified axisymmetric solution of the Navier-Stokes equation with an eddy-viscosity model for the turbulence. This has been widely used, for example in the WindFarmer code [14], and has been well validated against wind farm measurements at least in terms of 10-minute mean power production without requiring any further tuning of parameters. The Gaussian-shaped profile starts spreading from two diameters downstream, with a non-linear spreading rate which increases with turbulence intensity, as defined by the eddy viscosity term. A typical velocity deficit distribution is illustrated in *Figure 1*.

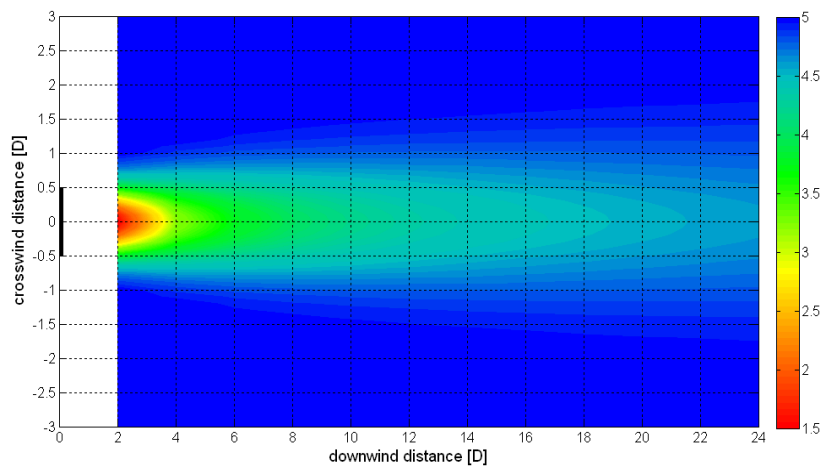


*Figure 1 – Example Ainslie wake deficit*

The wake is initialised two diameters (2D) downstream, with centreline deficit

$$\delta = C_T - 0.05 - ((16C_T - 0.5) I / 10) \quad (3)$$

for turbine thrust coefficient  $C_T$  and fractional turbulence intensity  $I$ . According to momentum conservation, the wake half-width  $B$  (in diameters) is related to the centreline deficit by

$$B = (3.56 C_T / (8\delta(1 - 0.5\delta)))^{0.5} \quad (4)$$

and this relationship always holds as the wake moves downstream, with  $\delta$  decreasing and  $B$  increasing, at a rate defined by the eddy viscosity which is a function of turbulence intensity. The deficit profile remains axisymmetric and Gaussian, the deficit at a distance  $y$  diameters from the centreline being

$$\delta(y) = \delta(0) \exp(-3.56 y^2 / B^2) \quad (5)$$

Different variants of the Ainslie model are also available. In particular, a modification to the eddy viscosity term which depends on atmospheric stability is described in Section 4. The effect of stability on wake effects is increasingly recognised as important for wind farm control applications.

An alternative Gaussian profile model developed at EPFL [21], [22], [23] has also been implemented. This model has been used quite widely, in particular in the open-source Floris code

[24], [25], but more recently it has been found to work better if some of the parameter values are adjusted empirically to fit different situations, so these parameters are user-specifiable in *LongSim*. Other slight differences, for example between the NREL and Delft versions of Floris, are also implemented as options in *LongSim*.

### 2.8.2 WAKE TURBULENCE

Both the wake development and the downstream turbine loads depend critically on the turbulence, and it is therefore important to predict the increase in turbulence caused by the wakes themselves.

As in WindFarmer [14], the Quarton-Ainslie model ([15], as modified in [16]) for added turbulence in the wake is used by default. A more theoretically-based model would be desirable as this is a completely empirical model, fitted to various measured datasets from wind tunnels and from now rather outdated wind farms in the field. However, validations of the WindFarmer model, which depends on it, continue to confirm its validity.

### 2.8.3 WAKE DEFLECTION

If the turbine is misaligned to the flow direction, momentum conservation dictates that the wake centreline will be deflected laterally. There will always be such yaw misalignments, since the turbine yaw control is not instantaneous but responds slowly to direction changes, due to, for example, low-pass filtering of the yaw misalignment, a hysteresis dead-band to ensure that yaw manoeuvres do not occur too frequently, and a slow yaw rate (typically a fraction of a degree per second). More importantly, yaw misalignments may also be commanded deliberately for the purposes of wake steering control, where the wind farm controller deliberately yaws turbines in order to steer their wakes away from downstream turbines. For both reasons, the model includes this wake lateral deflection effect.

Jímenez [19] derives a simple model for this effect, based on momentum conservation with a rectangular wake deficit profile, but the same model has been used for other wake profiles, e.g. in Gebraad [20], where the deflection recovery parameter has been tuned against CFD simulations. This Jímenez-Gebraad model has therefore been adopted as the default to use in combination with the Ainslie wake profile model. The somewhat more sophisticated lateral deflection part of the EPFL model [21], [22], [23] is also available, and is used as default if the EPFL wake profile is selected, although the profile and deflection models can also be mixed if desired.

### 2.8.4 WAKE SUPERPOSITION

The combined effect of two or more wakes on a downstream turbine is not yet well understood. Several models of wake superposition have been used in the literature. Different alternatives are available in *LongSim*, the default being the ‘dominant wake’ model used by WindFarmer [14], where only the highest velocity deficit and the highest added turbulence of all the wakes impinging on a turbine are used. The superposition model used by EPFL [21], [22], [23] is also implemented in *LongSim* – this uses a linear sum of absolute deficits, which may be more intuitive from the momentum conservation point of view. According to CFD calculations in [24], the dominant wake model works well for aligned turbines, while a linear combination of deficits may work better in cases where the wake centrelines are offset. Further work using CFD should help to define a more generalised model.

### 2.8.5 WAKE MEANDERING

The dynamic wake meandering model of Larsen *et al* [17] assumes that the wake is pushed around laterally and vertically by the low frequencies of the turbulence like a passive tracer, causing it to meander as it moves downstream. The low frequencies are defined in terms of spatial scales given by two “wake diameters”. For this application a constant scale is needed, and anyway the wake diameter is not explicitly defined, so the spatial scale has been made user-definable. It is used in generating the low-frequency wind field as described above, and the resulting low frequency wind speed variations are then used to define the movement of the wake centreline from one timestep to the next.

One complication here is that the parameterisation of the Ainslie wake deficit model has been calibrated against 10-minute average wind farm measurements. Presumably, wake meandering will have been occurring during each 10-minute sample, resulting in a mean wake deficit profile which will have been ‘smeared out’ laterally and vertically by the meandering. Therefore, the instantaneous wake deficit profile must be narrower and deeper than the 10-minute average profile. The time-domain simulation model requires the instantaneous profile, so a correction to the profile is made following a suggestion by Ainslie [13], who derives an expression for the reduced centreline deficit of the smeared-out profile,  $\delta'$ , as a function of the standard deviation of wind direction,  $\sigma_\theta$ , at downstream distance  $x$  (diameters):

$$\delta' = \delta / (1 + 7.12 * (\sigma_\theta x / B)^2)^{0.5} \quad (6)$$

Equation (4) still applies to the new profile, allowing its increased half-width  $B'$  to be calculated. However, since the Ainslie model has been parameterised against 10-minute data, it is already ‘smeared out’, so the inverse of this Ainslie correction must be applied to obtain the instantaneous profile which can then be allowed to meander. The ratio  $p = \delta' / \delta$  can be found as the solution to a quadratic:

$$p^2 + p [7.12 (\sigma_\theta x / B')^2 / (1 - 0.5\delta') - 1 - 3.56 \delta' (\sigma_\theta x / B')^2 / (1 - 0.5\delta')] \quad (7)$$

hence  $\delta = \delta' / p$ , and  $B$  is obtained from Equation (4).

If data for  $\sigma_\theta$  is not available, *LongSim* calculates a value assuming a fixed ratio between the lateral and longitudinal turbulence intensities (default 0.7).

When the model is run with this narrower profile, the meandering does indeed smear this out to produce the correct 10-minute mean profile, as shown in Figure 2, which plots the velocity profile in four wakes at a downstream location behind four turbines in two staggered rows. The original (smeared) steady-state wake profile from WindFarmer is shown by the solid line; the red circles are from the simulation model, using the smeared profile and no meandering; the green circles show the narrower (instantaneous) wakes obtained by applying the inverse Ainslie correction; and when meandering is applied to these, the deficit averaged over time is smeared out to give the purple squares.

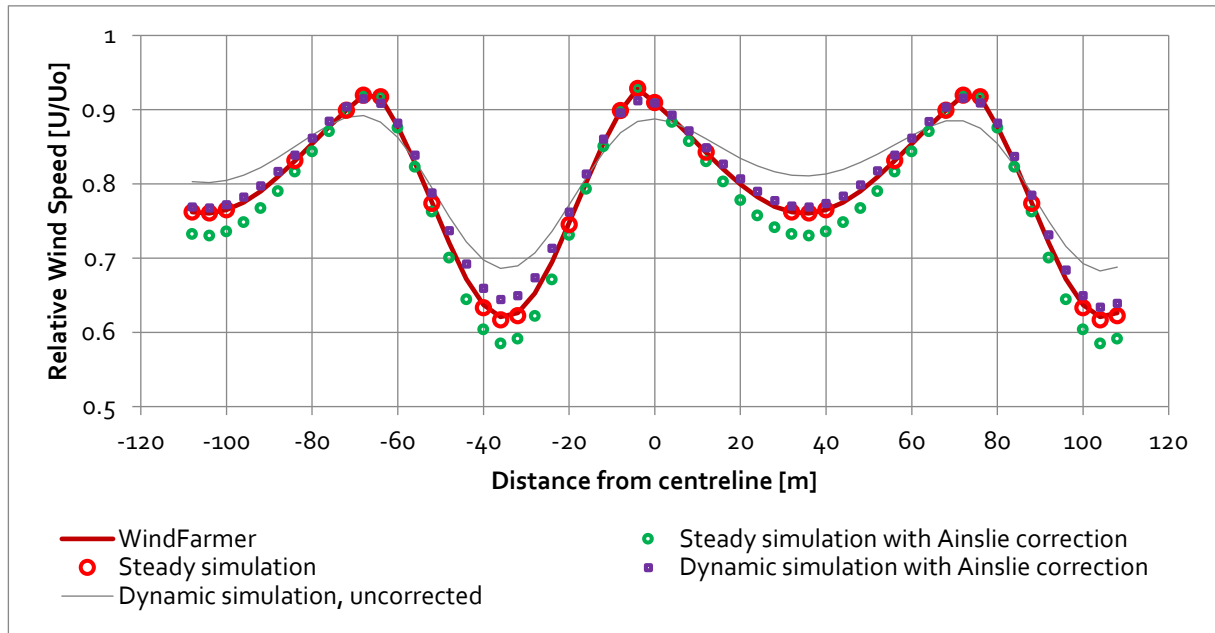


Figure 2: Ainslie meandering correction

## 2.8.6 WAKE ADVECTION

When a change to the wake profile occurs, whether by turbine control action or a change in wind conditions, this change must advect downstream. By analogy with wake meandering in the lateral and vertical directions, this advection is assumed to be driven by the longitudinal component of the low-frequency wind field. However, it is also likely that the reduced wind speed in the wake itself causes the mean wake advection speed to be lower than the free wind speed. There is little information available in the literature to quantify this effect; in [18] some results are reviewed, suggesting that the advection speed may be around 80% of the free wind speed, but that it also depends on turbulence and downstream distance. Two options are therefore provided for the mean advection speed, pending further work: a fixed fraction of the free wind speed, or a linear combination of free wind speed and mean speed within the wake profile.

## 2.9 WIND FARM CONTROL

*LongSim* includes a wind farm control module, which has access to model information such as would be expected to be available to a wind farm SCADA system, and outputs power delta and yaw misalignment set-points to all the turbines (and potentially other commands). This is flexibly implemented, to allow all kinds of wind farm control algorithms to be tested. It has currently been tested for a quasi-static open-loop or “advanced sector management” controller, with look-up tables defining the delta and yaw set-points as a function of farm wind speed, direction and turbulence intensity [27].

In practice these wind conditions must be estimated by the wind farm controller from available measurements. *LongSim* can use the smoothed time series coming from met mast measurements, with further low-pass filtering applied, but in practice a met mast may not be available, in which case turbine measurements are needed, which might in any case be better. *LongSim* therefore includes an algorithm to determine at each step which turbines are not waked by other turbines, and then averages the wind speed, direction and turbulence estimates from

all these turbines to obtain values which are assumed to be representative of the whole wind farm at that time.

The wind farm control module in *LongSim* can also be used for other purposes, for example to implement alternative centralised yaw control strategies at wind farm level, as in [28].

## 2.10 LONGSIM USAGE

*LongSim* can be used in three main ways:

- A steady-state calculation generates the wake field of the entire wind farm for a given uniform steady wind condition. The condition of each turbine is determined, allowing the total wind farm power to be calculated for that condition.
- An optimiser loops through many wind conditions, each time using the steady-state calculation iteratively to optimise wind farm control setpoints at all the turbines. This can include yaw offsets for wake steering, power delta setpoints for induction control, or both.
- Dynamic simulations can be run (with or without wind farm control, for example using the optimised setpoints) to generate time series giving the detailed performance of each turbine and the wind farm as whole in realistic varying wind conditions determined by wind fields described above. Simulations can be used to test wind turbine supervisory control as well as wind farm control. As well as time histories of power, pitch, rotor speed, yaw misalignment, etc., supervisory control outcomes such as total yaw travel or the number of yaw manoeuvres are logged. Long simulations can be run, to ensure that low-frequency wind variations and turbine and wake behaviours are properly represented.

### 3 VALIDATION DATA

Information from Lillgrund wind farm has been used in this report as a basis for validation of the *LongSim* model. The wind farm layout is shown in *Figure 3*

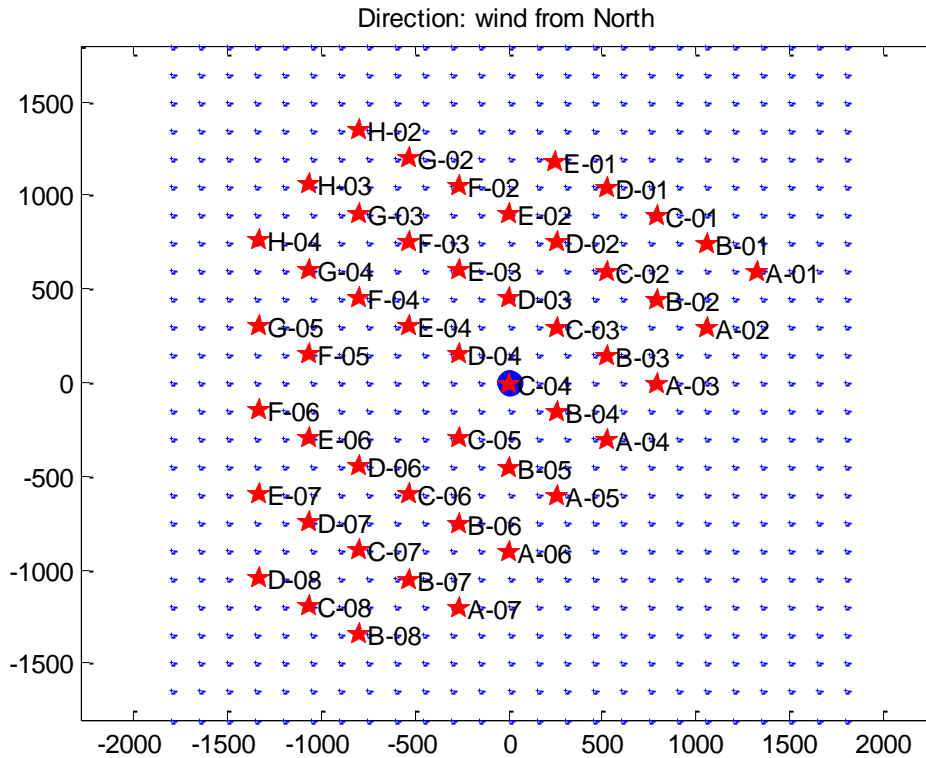


*Figure 3: Layout of Lillgrund wind farm*

#### 3.1 TURBINE INFORMATION

##### 3.1.1 TURBINE MODEL

The turbine information which was made available for use in this work consisted of blade geometry information and aerofoil polars, together with the following general information:

**Geometry:**

Hub radius	1.309 m
Blade length	45 m
Hub height	68.8 m
Tilt angle	5 deg
Cone angle	2.7 deg

**Operation:**

Rated power	2.3 MW
Minimum rotor speed	0.8 rad/s
Rated rotor speed	1.67 rad/s

Minimum pitch angle	-1.0 deg
Maximum pitch angle	90 deg
Generator efficiency	94%

This information was used to construct a model of the turbine to run in the aeroelastic code *Bladed*. This was used to generate steady power and thrust curves (as a function of wind speed) and coefficient tables of power and thrust coefficients (as a function of tip speed ratio and pitch angle). The latter would allow the rotor speed and pitch dynamics of the turbine to be modelled, but for that the torque and pitch control dynamics would also be required, and this information was not provided. Therefore, the *LongSim* simulations were run using the steady power and thrust curves, without the rotor speed and pitch degrees of freedom. This may result in some loss of fidelity in the time-domain simulations, particularly around the rated transition between torque and pitch control. Also the behaviour around cut-in could not be represented accurately. However, for simulations in the range between cut-in and rated wind speeds, the loss of fidelity is probably not severe.

*LongSim* also simulates the yaw dynamics of the turbines, which is important in conditions of changing wind direction. However, no yaw control information was provided. Therefore two options were available: either 'Ideal' yaw control, in which the turbine yaws continuously to follow the rotor-average wind direction exactly, maintaining zero yaw misalignment at all times, or an assumed model for the yaw control. The latter was chosen as being more realistic, so the following typical yaw control action was assumed:

- Yaw rate: 0.3 deg/s
- No yawing below 2.5 m/s wind speed
- Yaw error filter time constant: 30s (applied to the estimated wind direction, made up of nacelle position plus wind vane misalignment, in order to avoid slow filter response when the turbine yaws)
- Yawing starts when the filtered yaw error exceeds 8 degrees
- Yawing stops when the filtered yaw error reaches zero

### 3.1.2 EFFECT OF YAW MISALIGNMENT

The effect of yaw misalignment on the power and thrust curves can be calculated by *Bladed*. For the purposes of this validation exercise, however, yaw misalignments have been assumed to be kept reasonably small by the assumed yaw control logic, and so a simple algorithmic yaw correction has been applied instead, to save time.

The simple assumption that power decreases as  $\cos^3(\text{yaw})$  seems not to be valid, and a number of cases have demonstrated a factor of  $\cos^p(\text{yaw})$  with the exponent  $n$  being much less than 3, typically more like 1.4 – 2.0 (e.g.  $p=1.43$  in [29]). Here the value  $p=1.4$  has been used as a basis; however, this cannot simply be used to scale the entire power curve, as it would result in less than rated power in high winds where, in reality, pitch control would compensate for yaw to bring the power back to rated. Therefore, a factor  $\cos^w(\text{yaw})$  has instead been applied to the wind speed used for the power curve look-up. For this turbine,  $w = 0.5$  has been used as it gives a very similar result to  $p=1.4$  in below-rated wind speeds while allowing the power curve still to reach rated, albeit at a higher wind speed than at zero yaw. The resulting power curves are illustrated in *Figure 4* for two different yaw angles. For the turbine thrust look-up, the same factor  $w$  is assumed to apply to the effective wind speed.

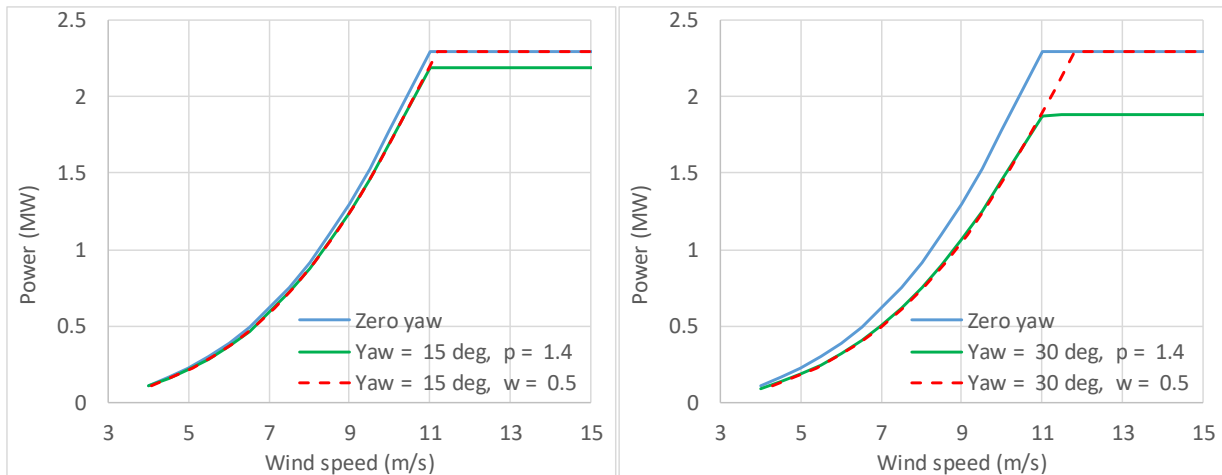


Figure 4: Assumed effect of yaw misalignment on power curve

### 3.2 SCADA DATA

The raw SCADA data consisting of signals sampled at each turbine at irregular intervals, typically a few seconds, was provided. This data format allows to reduce the storage volume required since a new record is written whenever the value of the signal changes. Each recorded signal was processed and averaged into 5-minute averages for a period covering the whole month of March 2012, and this was used for the analysis described in this report. A second batch of files was provided at a later stage, including the same SCADA signals with continuous signal recording every 10 seconds (or 0.1 Hz). This new dataset was not utilised for the study presented here, but further analyses are being planned to address any concern that might arise from the different sampling frequency of the different datasets.

The signals used here, for each turbine, were the wind speed mean and standard deviation, nacelle direction mean and standard deviation, and active power mean. Some curtailment information was also made available for all the turbines subjected to curtailment. The information consists of time-series of the curtailment-mode identifiers. However, details about each curtailment mode (i.e. the correspondent power and thrust curves) were not provided up to the time of issue of this report.

It became apparent during the analysis that the data was not calibrated and still contained many imperfections, and that significant effort would be needed to clean it up. This significantly impairs the detailed comparisons between the SCADA data and the LongSim model which had been envisaged, as explained below.

### 3.3 METEOROLOGICAL DATA

Unfortunately, no concurrent meteorological data is available as part of this project and it is therefore not possible to pair SCADA data from the operational turbines to concurrent statistics of the wind inflow. The main wind statistics are therefore obtained from the turbines' SCADA data, as described in the previous section. In order to characterise the atmospheric stability at the wind farm site, nonconcurrent data from the nearby Drogden Lighthouse were provided.

### 3.3.1 METEOROLOGICAL DATA FROM THE DROGDEN LIGHTHOUSE

The Drogden Lighthouse is located approximately between 5.1 and 6.3 km to the north-west of the Lillgrund wind turbines. Signals recorded at the lighthouse were not available to all the Total Control partners due to permission issues; however, DTU provided the time-series of Obukhov lengths obtained from the lighthouse signals, along with some wind speeds and wind direction signals from calibrated nacelle-mounted instruments from nearby turbines. The provided time-series of Obukhov lengths, extending between 26-05-2008 and 22-08-2011 with a 10-minutes averaging period, have been obtained using AMOK, a tool developed by DTU to classify the atmospheric stability from meteorological measurements. Details about this methodology are provided in [30]. The wind speed, wind direction and air temperature at 22 m above the sea level (a.s.l.) along with the water temperature have been used to estimate the Obukhov length.

### 3.3.2 CHARACTERISATION OF THE ATMOSPHERIC STABILITY AT THE SITE

As clarified above, the 5-minutes averaged SCADA data, extending for the whole month of March 2012, have been used for the simulations discussed in this report. As a preliminary check, the wind rose at different wind turbine locations was calculated to identify the prevailing wind direction and, therefore, the directional wind sector with the highest data coverage. As shown in *Figure 5*,  $300^\circ$  is consistently indicated as the prevailing wind direction at all the four turbine locations. Turbine D08 was selected as a reference turbine for the estimation of meteorological conditions for the entire wind farm, as it remains undisturbed by other turbine wakes for all wind directions which were recorded during the one-month data.

The occurrence of different atmospheric stability classes has been investigated by visualising the change of the Obukhov length. In *Figure 6* the histograms of neutral, stable and unstable Obukhov lengths are presented, showing the occurrence of non-neutral conditions is non-negligible across the approximately 3 years of data. The median values of the Obukhov length for the three distributions have been calculated for different filtering sets, based on different wind speed and wind direction, and they have been found to be roughly equal to -105 m, 1200 m and 100 m respectively for the unstable, neutral and stable cases. This is also shown for different hours of the day in *Figure 7*, where a time-dependent pattern for stable and unstable atmospheric stratification emerges. If a correlation is assumed between atmospheric stratification and hour of the day, this should correspond to specific patterns of wind speed and turbulence intensity variations as seen from the turbine SCADA data, even if not recorded during the same period: this is shown in *Figure 8*, where periods of high wind speeds and low turbulence intensity at the reference turbine D08 are visible during the hours when a high occurrence of stable atmospheric conditions are recorded at the lighthouse. What is more, due to the vicinity of the wind farm to the coast of Denmark (from southwest to northwest) and Sweden (from north to southeast), the presence of coastal effects has also been assessed for the prevailing  $300^\circ \pm 15^\circ$  wind direction. After filtering the time-series of Obukhov lengths by wind directions, a clear prevalence of unstable atmospheric conditions appears during the hours of the night and morning, whereas stable atmospheric conditions appear dominating in the afternoon, and with neutral conditions reaching high occurrence from the late morning to the evening, as shown in *Figure 9*.

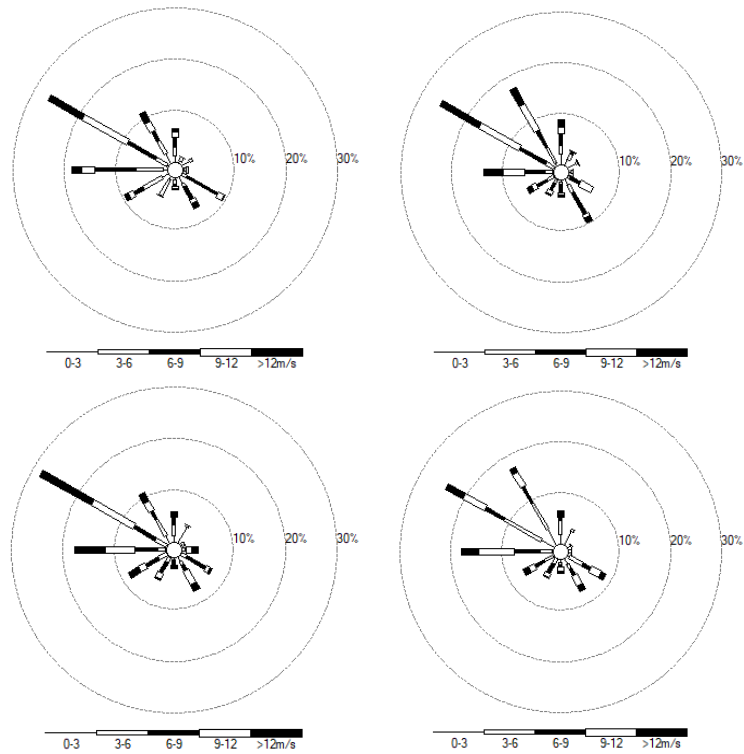


Figure 5: Wind rose calculated for the month of March 2012 at four turbine locations: (from top to right and from left to right) E01, H08, D08, C08.

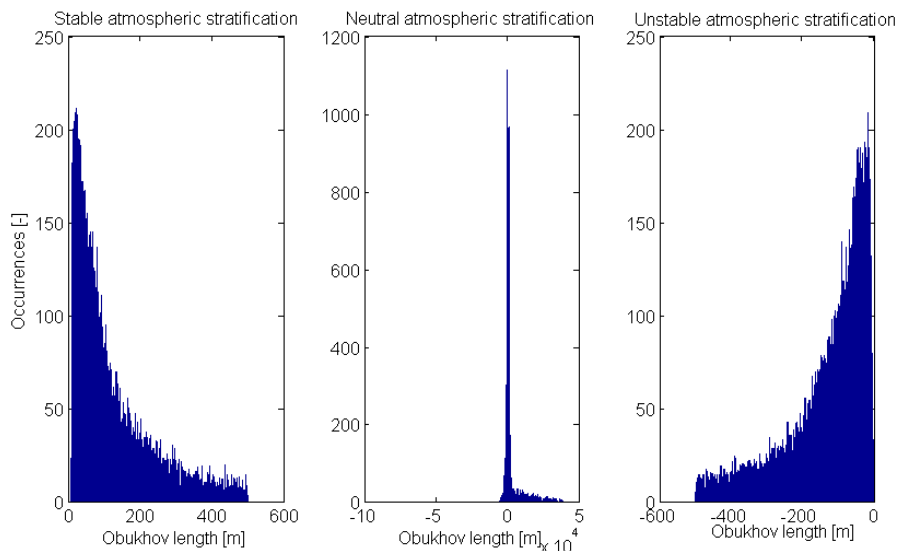


Figure 6: Histogram of occurrences of neutral, stable and unstable atmospheric conditions, based on the estimated Obukhov lengths (all-directional and for wind speeds between 3 and 15 m/s).

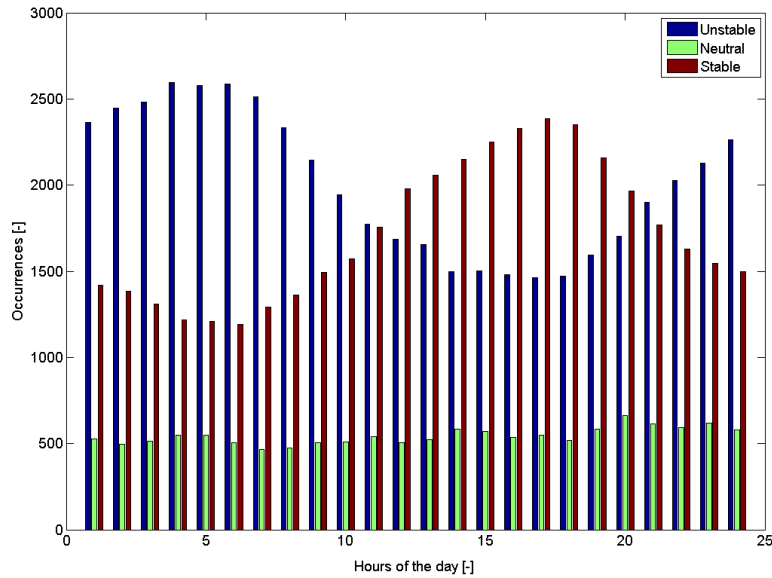


Figure 7: Histogram of occurrences of neutral, stable and unstable atmospheric conditions, based on the estimated Obukhov lengths, versus time of day (all-directional and for wind speeds between 3 and 15 m/s).

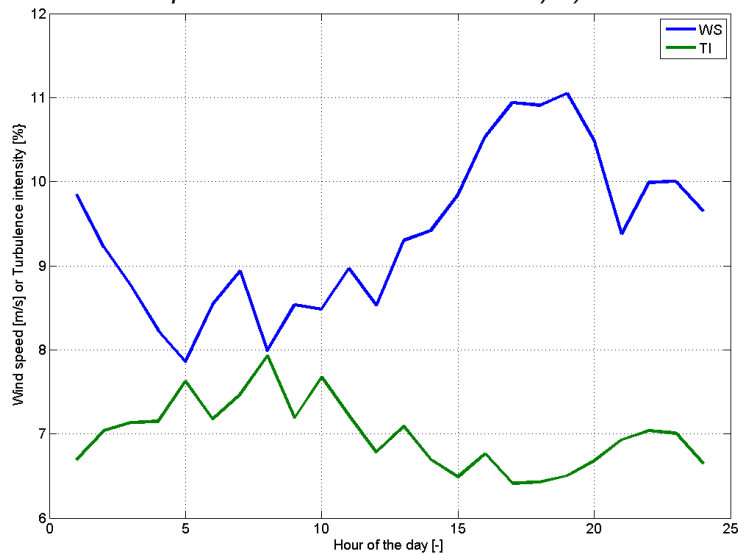


Figure 8: Average wind speed and turbulence intensity at turbine D08 for the whole month of March 2012, versus time of day (all-directional and for wind speeds between 3 and 15 m/s).

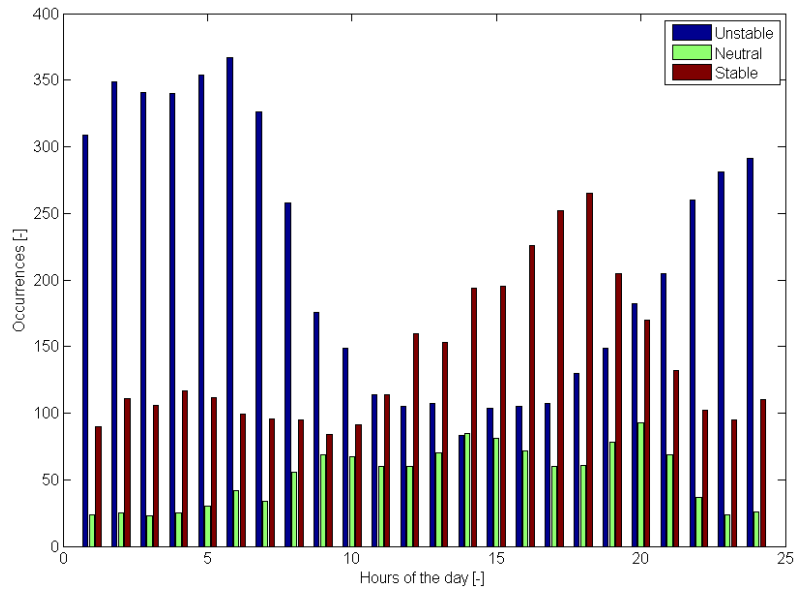


Figure 9: Histogram of occurrences of neutral, stable and unstable atmospheric conditions, based on the estimated Obukhov lengths at the  $300^{\circ}\pm 15^{\circ}$  wind direction sector, and filtered for wind speeds between 3 and 15 m/s.

## 4 WAKE MODEL VALIDATION

### 4.1 WAKE MODELLING AND ATMOSPHERIC STABILITY

In Section 2.8 an introduction to the Gaussian engineering wake models used in *LongSim* is given. One of the main drawbacks of such models is that they do assume atmospheric neutral conditions and therefore are not able to correctly predict the wake deficit for stable or unstable conditions. Other models currently used with particular focus on the offshore market, like DTU's FUGA, do take the atmospheric stratification into account.

For the purpose of modelling the turbine wakes in specific periods characterised by stable or unstable conditions, an experimental model has been used for this analysis. This is based on recent internal research by DNV GL and is pending publication [31].

This model is based on a modification of the eddy viscosity term in the Ainslie model, by which a correction factor is introduced. This correction is based on the Businger-Dyer empirical theory for non-neutral wind profiles, and the experimental parameters used in this model are the ones proposed by Högström [32],[33].

Wind farm production data has been used to validate this model and two examples are shown in *Figure 10*: in the Wieringermeer test case the Obukhov length used in the model was estimated from concurrent mast data for two different periods; in the Nysted test case, the Obukhov length was estimated from previously-estimated occurrence probability of stability-classes. For the Nysted case, the Crespo-Herandez model for wake added turbulence [33] was used, along with the sum-of-deficits superposition model.

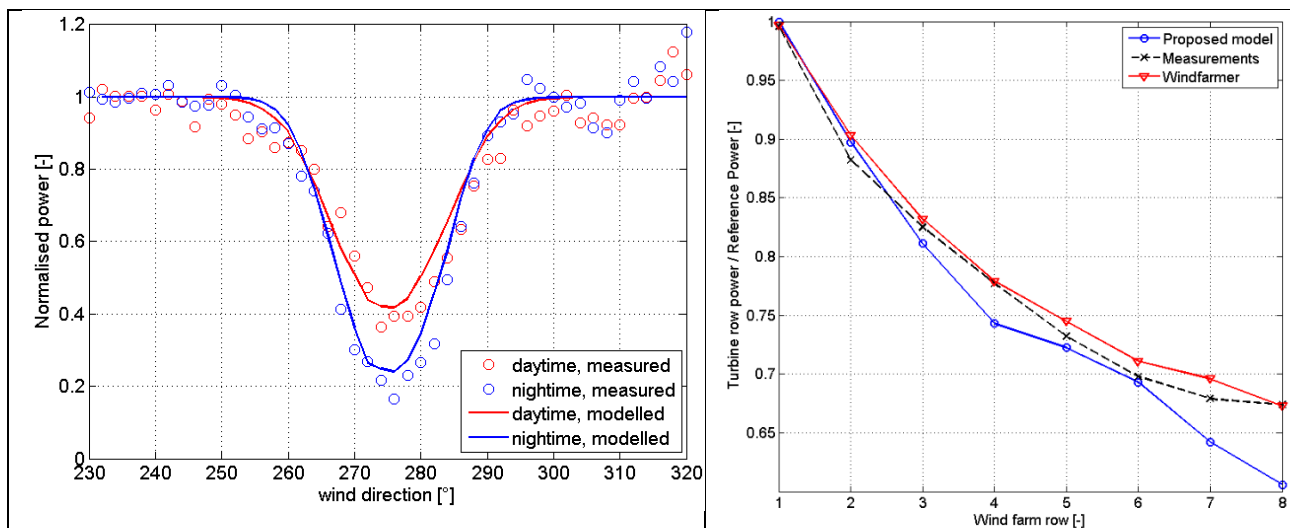


*Figure 10*: Examples of wind farm data validation using the 'modified Ainslie model' proposed in [31]. (Left) Wieringermeer wind farm validation case, (right) Nysted wind farm validation case,

#### 4.1.1 INPUTS AND WAKE MODELS USED

A series of steady-state simulations have been carried out with different wake models, and their results compared to measured production data at the Lillgrund wind farm. The results from each

of these models were used to better inform the dynamic simulations that will be discussed in Chapter 5.

All the steady-state simulations have been run for a specific wind speed, wind direction and turbulence intensity:

Wind direction: As previously explained, it was chosen to focus on the 300° wind direction sector. In order to be able to perform closer comparisons with the results of the dynamic simulations, a narrow directional bin width of 5° was chosen. Steady-state simulations were also performed with directional bins of 30° to better compare the wake models used, as it will be shown in the next sections.

Wind speed: It was decided to run the simulations focusing at a wind speed bin between 8.5 and 9.5 m/s, since being the most frequent wind speed bin in the limited-sized set of SCADA data.

Turbulence Intensity: The SCADA data included turbulence intensity as standard deviation of the 5-minutes averaged wind speeds. However, the wind speed measurements are taken behind the rotor and are therefore subjected to turbulent airflow. Although different methodologies have been tested on the provided Lillgrund SCADA data, based on the existing literature for the estimation of turbulence intensity from turbine production data [35] and [36], unclear results were obtained. Therefore, the turbulence intensity from the SCADA data was used for the current analysis.

As will be detailed in Chapter 5, the authors have some concerns with the quality of the provided raw SCADA data, as they are not calibrated and hence show large deviations from what is expected. To better represent the variation of power production data across the wind farm, the power from the SCADA data is shown in *Figure 11*. It can be noticed how, for winds blowing from the 300° direction (relative to the reference turbine D08), the power at the turbines along the westerly perimeter exhibits a decrease, potentially indicating a decrease in wind speeds from south to north. To easily identify the turbines which are affected by any curtailment scenario, the labels of such turbines have been coloured in pink. In order to check for any bias in wake modelling discussed in this section, the variation of power median from the SCADA signal was calculated both including and excluding the SCADA records which indicated any curtailed operational mode (i.e. different than zero). Using the filters already described based on wind speed and wind direction at the turbine D08, the total number of records is 8916, and only 734 entries are flagged as curtailed production. If all the records are kept, a median power of 1064 kW is obtained, against the median power of 1095 kW obtained when ignoring the curtailed production records. It is therefore considered that curtailment has no considerable effects for the operational period considered.

To further investigate the variations of SCADA measurements, in *Figure 12* the median wind speeds calculated from the filtered data is shown, along with the difference between the wind speed from the SCADA data and the wind speed back-calculated from the SCADA power. The difference between the two indicative wind speeds can be relatively high for many of the Lillgrund wind turbines.

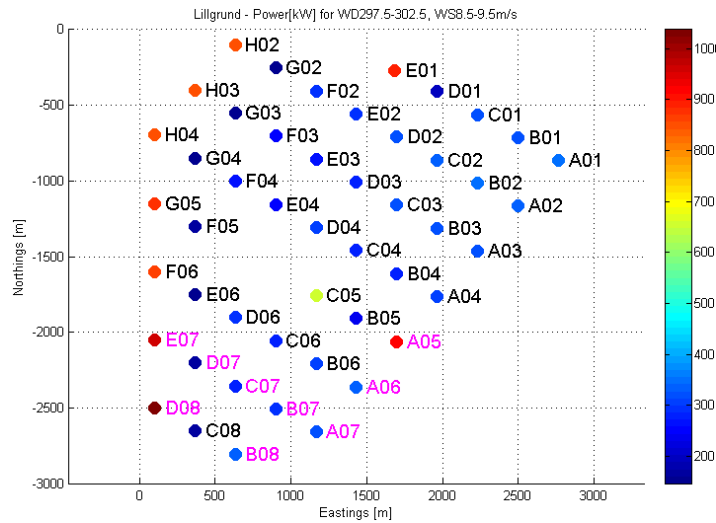


Figure 11: Median of power from SCADA data for the whole month of March 2012. Filtering on turbine D08: wind speed from SCADA signal between 8.5 and 9.5 m/s, Wind direction within the  $300^{\circ} \pm 2.5^{\circ}$  range. Curtailed wind turbines labelled in pink.

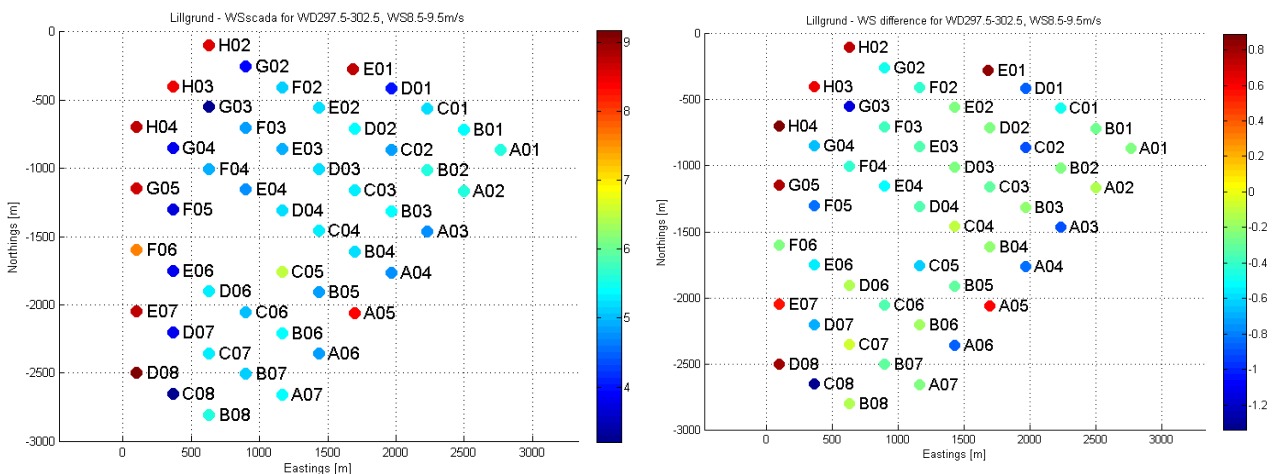


Figure 12: (Left) Median of wind speed from SCADA for the whole month of March 2012. Filtering on turbine D08: wind speed from SCADA signal between 8.5 and 9.5 m/s, Wind direction within the  $300^{\circ} \pm 2.5^{\circ}$  range. (Right) Difference between the wind speed from the SCADA signal and the wind speed back-calculated from the SCADA power signal.

#### 4.1.2 RESULTS FROM STEADY-STATE WAKE MODELLING AT THE LILLGRUND OFFSHORE SITE

The models used in these comparisons are:

- Windfarmer model (also labelled 'Ainslie LWF' in some plots): this model includes adjustments to model deep array effects [37]. This also uses the Quarton-Ainslie added turbulence model [15] and the Dominant-wake superposition model by default.
- Modified Ainslie model: this model has been described in the previous section and it has been run with three different setups, that is using three different Obukhov lengths representative of unstable, neutral and stable atmospheric conditions, respectively. The Obukhov lengths specifically used for the three models were based on the data derived

from the lighthouse, after filtering for wind directions  $300^{\circ} \pm 15^{\circ}$  and wind speed between 8.5 and 9.5 m/s, obtaining approximated values of the Obukhov length of -105 m, 1000 m and 100 m for the three stability classes. Also, this model uses the Quarton-Ainslie added turbulence model and the Sum-of-Deficits model for wake superposition: these choices are justified in the pending publication [31].

Additionally, the weighted average of the unstable, neutral and stable models results have been used for the final comparisons.

The comparison against SCADA data was performed on a row-by-row basis, to better visualise the effect of wake development within the wind farm array. Preliminary investigations were carried out on the southernmost column of three turbines, D08, C08 and B08.

A large discrepancy between measured data and model results was found when the models were initiated using the wind speed used as reference for turbine D08, i.e. 9 m/s. As shown in *Figure 13*, the modelled power production showed a large overprediction at turbine D08, indicating either a wrong power curve used in the model or a wrong wind speed indicated by the SCADA data. Given the large difference shown in the comparison above, all the plots below are based on the power-derived inflow wind speed.

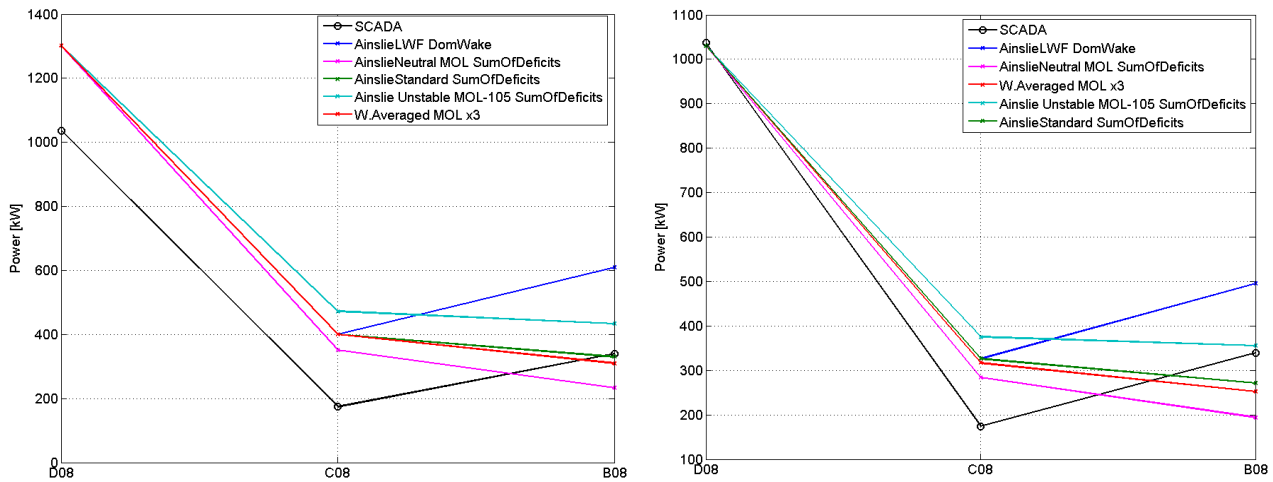


*Figure 13:* Power production modelled at turbines D08, C08 and B08. The modelled power is shown for 9 m/s inflow wind speed (left) and for the median wind speed calculated from the measured power production, 8.3 m/s.

The wake models' comparisons were performed on a row-by-row basis and the results are shown in *Figure 14* and *Figure 15*. The results are shown for the case where no time-of-day filtering was applied as well as for the case where a filter for hours between 21 and 8 only was applied, in order to try and isolate the occurrences with prevalent unstable atmospheric conditions, based on the estimate shown in *Figure 9*.

For both these cases, it can be noticed how all the models considered tend to underestimate the wake effects at the second turbine in each row, with the exception of the modified-Ainslie model set up with an Obukhov length characteristic of strong atmospheric stability; however, this is deemed not to be a realistic behaviour for the filtered dataset used for these comparisons. For all the other turbines in each row, it can be noticed how both the Windfarmer model and the modified-Ainslie model for unstable conditions tend to perform quite similarly, and broadly manage to agree with the measurements, especially for rows 3, 4, 6 and 7. The modified-Ainslie model for unstable conditions manages to agree reasonably well also with the measured power at turbine C05, adjacent to the empty area in the middle of the wind farm.

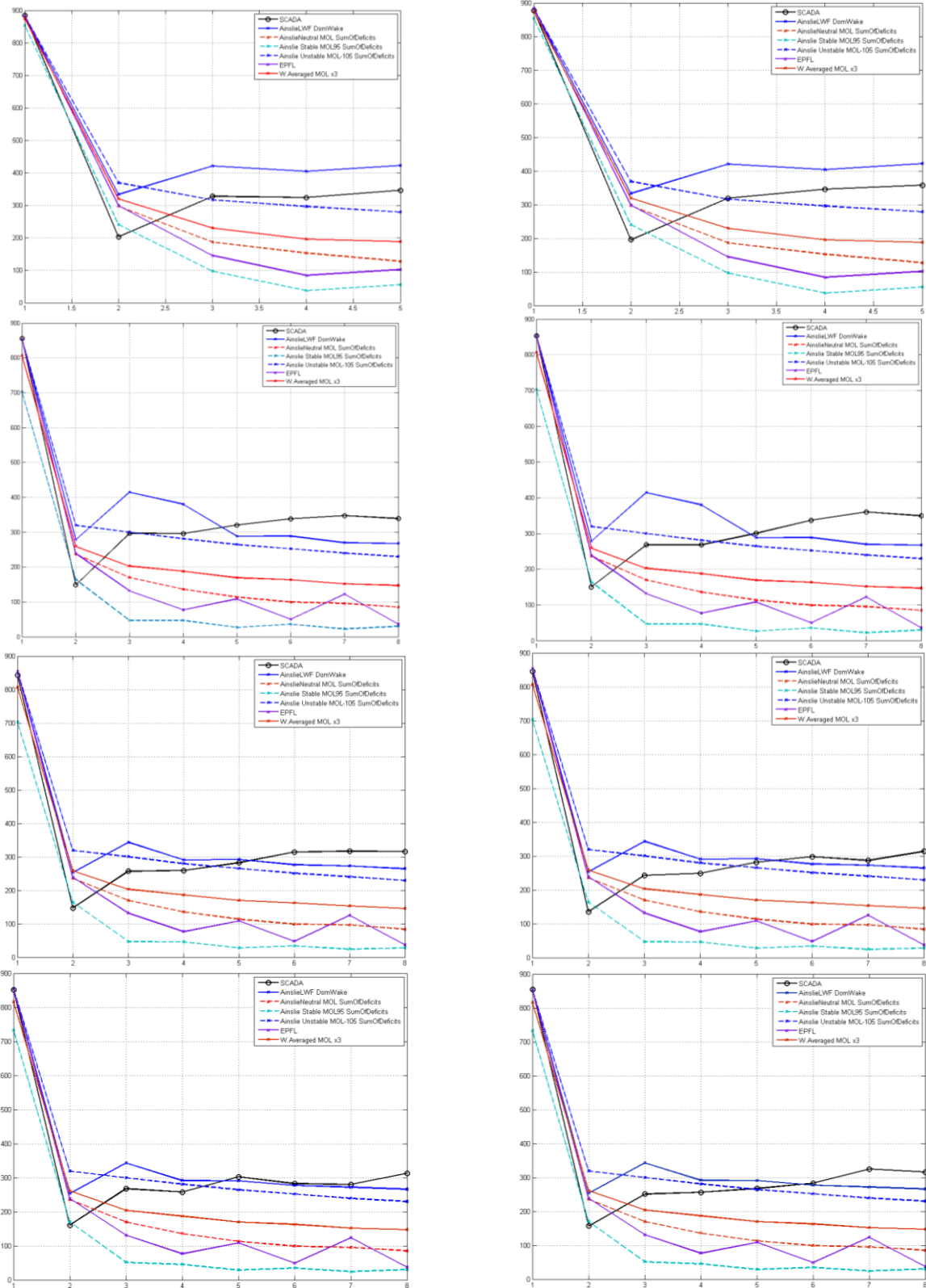


Figure 14: Power production modelled at each wind farm row for wind directions within the  $300^{\circ} \pm 2.5^{\circ}$  range. Different models' predictions are compared to the SCADA data for (left) all-day data and (right) hours between 21 and 8 (i.e. predominantly unstable conditions). Wind farm rows 1, 2, 3 and 4 from top to bottom.

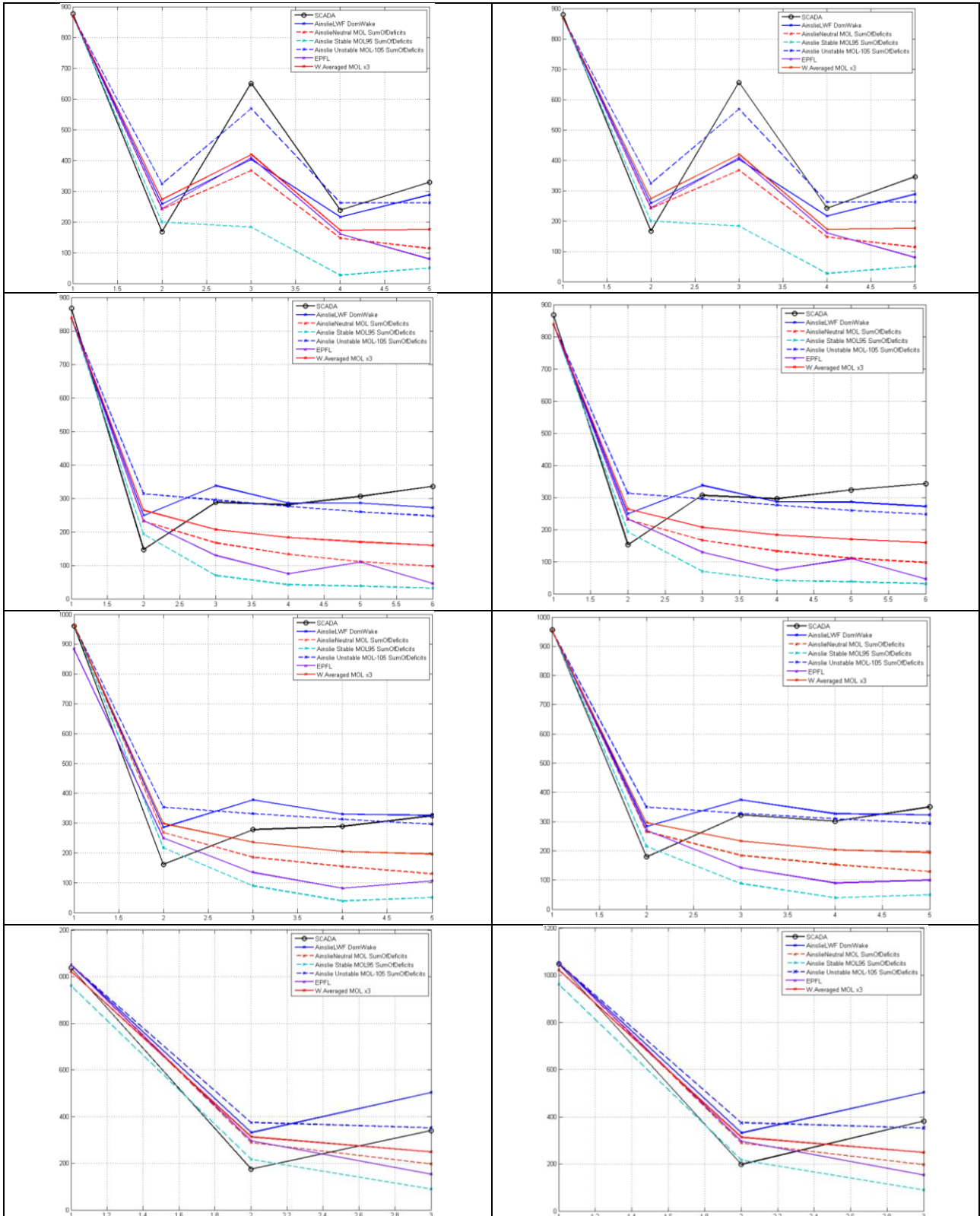
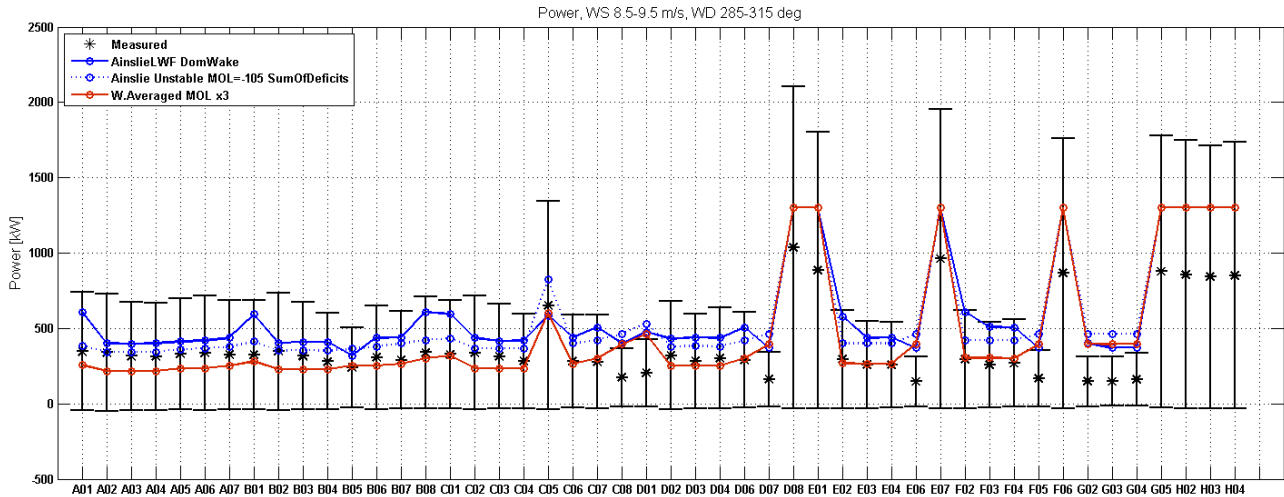
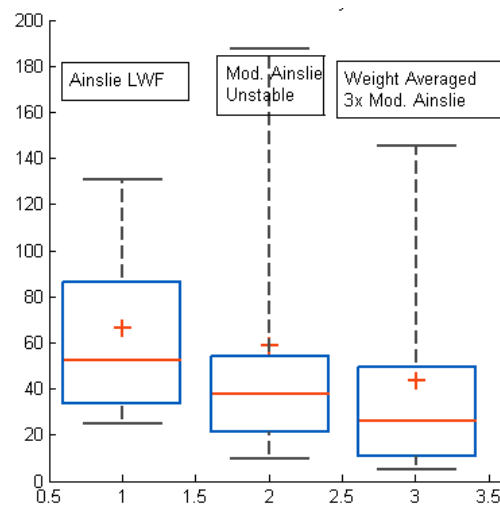


Figure 15: Power production modelled at each wind farm row for wind directions within the  $300^{\circ} \pm 2.5^{\circ}$  range. Different models' predictions are compared to the SCADA data for (left) all-day data and (right) hours between 21 and 8 (i.e. predominantly unstable conditions). Wind farm rows 5, 6, 7 and 8 from top to bottom.

Comparisons of different wake models for such narrow wind directions could introduce bias towards the dominant-wake superposition model, whereas larger directional bins are considered to be preferable for these comparisons, as the influence of turbines in adjacent rows could affect the interaction of wakes. Therefore, a wake model comparison was performed for a larger  $300^\circ \pm 15^\circ$  wind direction sector. These comparisons are shown in *Figure 16*, where no time-of-day filtering was applied.



*Figure 16:* Power production modelled using three different models, compared to power productions from SCADA data, performed with a  $300^\circ \pm 15^\circ$  wind direction sector. No time-of-day filtering.



*Figure 17:* Wake model errors (%); — 25th & 75th percentiles, — median, + mean.

The absolute error for each turbine between the predicted power (for each model) and the measured power was calculated. To better compare the overall prediction error of the three models, the box-plots of the turbine-wise errors are shown in *Figure 17*. It can be seen how both the modified-Ainslie model for unstable flows and the weighted-average of the stable, neutral and unstable modified-Ainslie models predict a median error lower than the Windfarmer error,

which is based on the assumption of neutral atmospheric conditions. This might suggest that the overall good performance of the Windfarmer model in the narrow wind direction bin tests be derived from the bias toward the dominant-wake superposition assumption (used in this wake model) which might perform better than the sum-of-deficit wake superposition model used in the other wake models. However, this cannot be demonstrated in this study.

It needs to be underlined that this wind farm has an inter-turbine spacing of approximately 3.3 rotor diameters, which is considered to be very small. The wake model comparisons considered here might be heavily affected by such a small inter-turbine spacing and therefore the relatively large errors in wake predictions could be explained by this factor.

As a final note, it is considered that the large uncertainties highlighted on the quality of the non-calibrated SCADA data, used for these comparisons, will affect these results.

## 5 DYNAMIC SIMULATION

### 5.1 INTRODUCTION

The comparison between *LongSim* and the SCADA data could potentially be done at different levels. Section 4 describes a comparison at the steady-state level, for evaluating the performance of different wake models when applied to Lillgrund wind farm. This section attempts to demonstrate that the time-domain simulation capabilities of *LongSim* are suitable for wind farm control design and testing, by running time-domain simulations which can be compared in detail against the SCADA data.

The first challenge is that the wind field used in the simulation can never exactly match the real wind field at every point during the period. Using actual measured wind speeds at each turbine is not particularly useful, as it would have no predictive capability. More useful is to generate a wind field with the correct statistical properties, and compare the results between SCADA and simulation on a suitable statistical basis. Met mast data concurrent with the turbine SCADA data would be a suitable basis for generating such a wind field, but there is no met mast available at this site. Therefore, data from one selected turbine has been used as if it was from a met mast. Turbine D-08 was selected, as it remains undisturbed by other turbine wakes for all wind directions which were recorded during the one-month data period which was selected (see section 3.2).

Different wind field realisations were generated from this turbine data by using different random number seeds. Simulations were then run using these wind fields, and the simulated performance of each turbine and of the wind farm as a whole was compared to the full set of SCADA data for this period. The detailed, point-by-point behaviour of each turbine cannot be matched to the SCADA data for each time instant, because the simulated wind field will not be the same as the actual wind field during the measurement period. However, it would be hoped that the spread of behaviours using different random number seeds should encompass the measured data, without any obvious systematic discrepancies.

Other aspects of the model dynamics which could be validated using fast SCADA data include the assumptions about wake advection. This would entail searching for distinct events in which the thrust of a (preferably unwaked) turbine changes suddenly, and trying to detect the time taken for the change in wake properties to be detected at downstream turbines. Short sequences of fast SCADA data could also be used to characterise the effect of wake meandering from an upstream turbine on the power of a downstream turbine, to validate in more detail the way in which wake meandering is modelled. However, the results presented below highlight some significant problems with the SCADA data which should be tackled before any such more detailed validation can be attempted.

### 5.2 WIND FIELD GENERATION

While the whole month-long period of SCADA data could be used to run one long simulation, it is more practical to run shorter simulations, at least initially, to gain confidence. Therefore, a number of sub-periods were selected which contained significant variation in wind speeds and directions, with the wind speeds mostly remaining above cut-in and below or around rated wind speed, as this range is of the most interest for wind farm control.

One such period (referred to as ‘Period 6’) was selected to provide the illustrative results in the next section, where the results of a very preliminary simulation are presented. The wind speed, direction and turbulence intensity for this 4.5-hour period are shown in *Figure 18*.

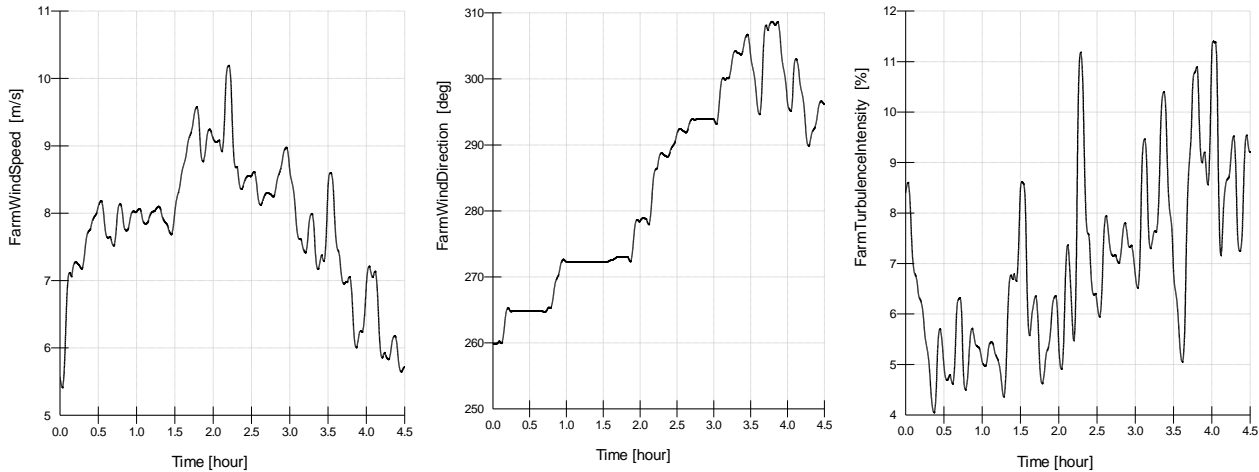


*Figure 18: Wind conditions for ‘Period 6’*

These wind conditions (together with wind direction standard deviation, not shown) were used, together with an assumed Kaimal spectrum of turbulence and a model for wind field coherence, to generate two different wind farm wind fields, with different random number generator seeds.

A number of other data periods were also used to generate wind fields in the same way. A longer period of about 10 hours, ‘Period 2’, was used for the further simulations which are presented in Section 5.4.

### 5.3 INITIAL RESULTS

Some initial results are illustrated here using the ‘Period 6’ wind field with seed 1, together with the unstable wake model with Obukhov length  $L = -105\text{m}$ .

The first thing to notice is that there are clearly problems with the nacelle direction sensor signals. These are clearly not well calibrated, with offsets between turbines of tens of degrees. The SCADA nacelle directions for the period are plotted in *Figure 19*. The blue line is for the reference turbine D-08, which fortunately seems to be fairly well in the middle of the range, at least for the first three hours, with other sensors generally recording within about 15 – 20 degrees of this signal. One turbine (G-05) is reading about 42 degrees less than D-08 on average. These differences are probably caused by poor calibration of the nacelle position sensor, which is not usually a very critical sensor, as the turbines would still be yawed correctly by the wind vane, but there is also a possibility of a wind vane calibration error, which would mean that the turbine really is running off-wind. Of course, it is possible that wake effects may cause some change in direction, but that would be a much smaller effect, and the largest difference is at C-05 which is never waked during this period.

Figure 20 shows the mean direction for each turbine over the period.

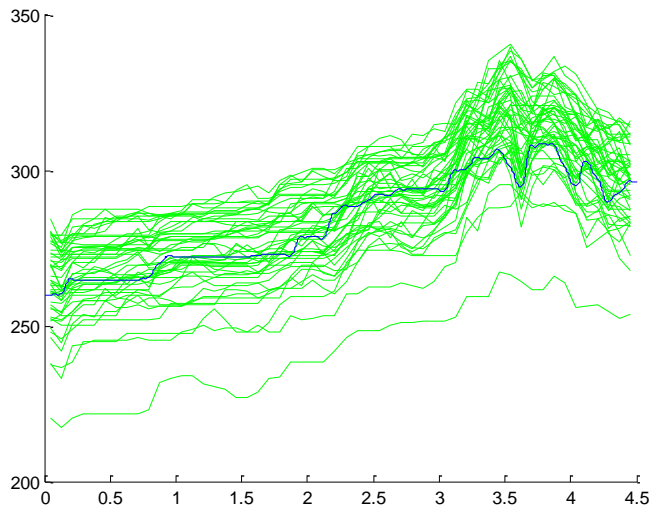


Figure 19: Nacelle directions in SCADA data: time histories

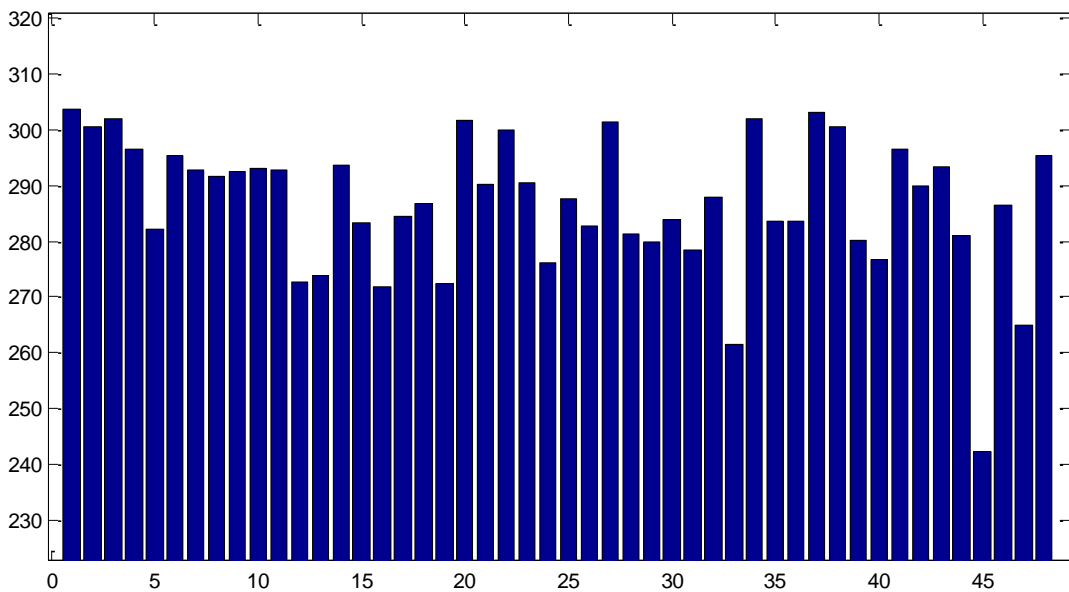
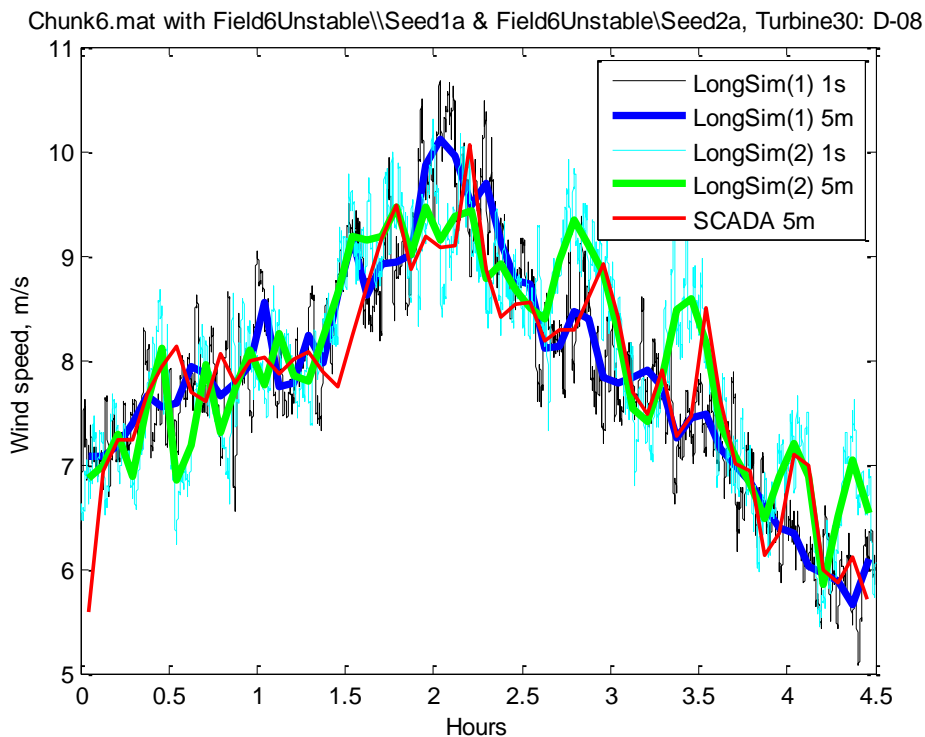


Figure 20: Nacelle directions in SCADA data: Means over period

Looking now at the reference turbine itself, D-08, which of course is never waked during this period, *Figure 21* compares the 1-second *LongSim* rotor-average wind speed time history, for two different random number seeds, against the 5-minute average SCADA data for this turbine which was used to generate the wind field. The thin lines give the 1-second simulated data, and the thick lines show the 5-minute averages. The 5-minute SCADA data is shown in red. The synthetic turbulence generated by *LongSim* is clearly visible. The 5-minute average wind speeds from *LongSim* follow the SCADA data well, as expected – they are not expected to be identical because of the added turbulence, and also because the SCADA wind data was actually applied at the centre of the wind farm (close to turbine C-04) and D-08 is at a different point in the wind field.

A similar plot for wind direction is shown in *Figure 22*, also showing a good correspondence to the SCADA data. The relative size of direction fluctuations is smaller compared to the overall variation in direction, so it is easier to see that the SCADA data actually lags the D-08 direction slightly, because D-08 is upstream of the reference point where the wind data is applied (the large blue dot in *Figure 3*). As can be seen from this figure, for westerly winds, D-08 is around 1500m upstream of the reference point, which corresponds to a time delay of around 0.05 hours given the mean wind speed of around 8 m/s, and the delay would become shorter as the direction swings more to the North-West. *Figure 22* confirms this very satisfactorily, which indicates that that the modelling assumption that changes in direction advect with the mean wind speed is a very reasonable one.



*Figure 21: Wind speed at the reference turbine (two seeds in LongSim)*

Turning now to the turbine power shown in *Figure 23*, we see a clear discrepancy, with *LongSim* predicting significantly more power than the SCADA data shows. Since the turbine remains unaffected by wakes for the entire period, the discrepancy cannot be due to the wake modelling. *Figure 24* plots the power against wind speed, and it is clear that the *LongSim* results follow the expected steady power curve well, indicating that either the turbine in reality is under-performing compared to this expected power curve, or that some form of curtailment might be applied, or that the SCADA wind speed measurement is inaccurate. No information has been provided regarding the origin of the SCADA wind speed measurement, for example whether it is the raw anemometer signal, whether it is corrected in any way for being behind the rotor, or whether it is a wind speed estimate from the controller.

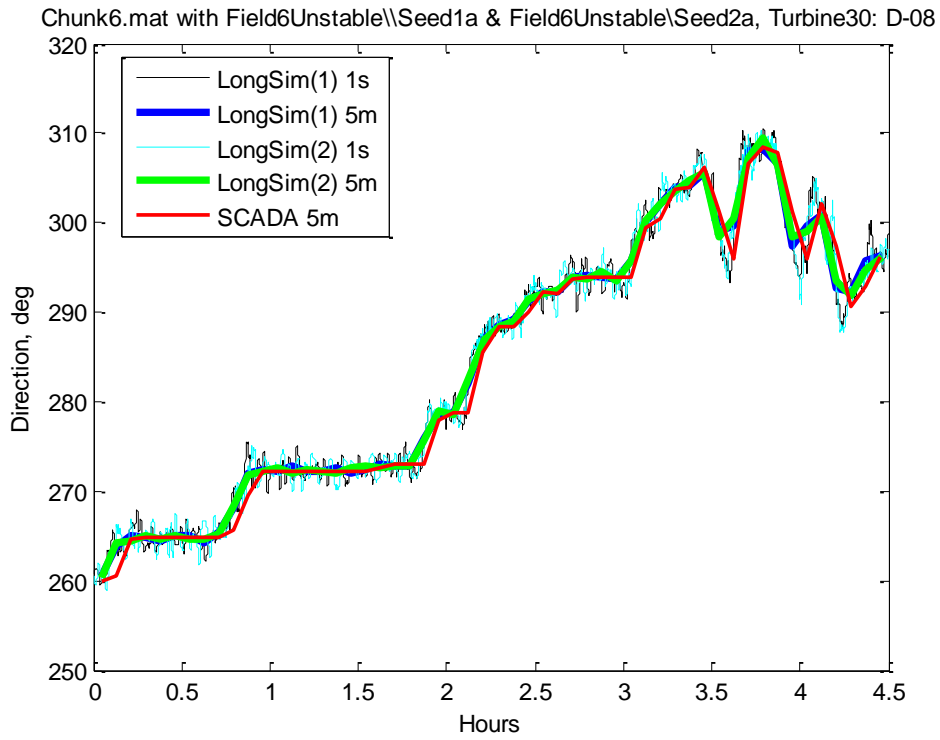


Figure 22: Wind direction at the reference turbine (two seeds in LongSim)

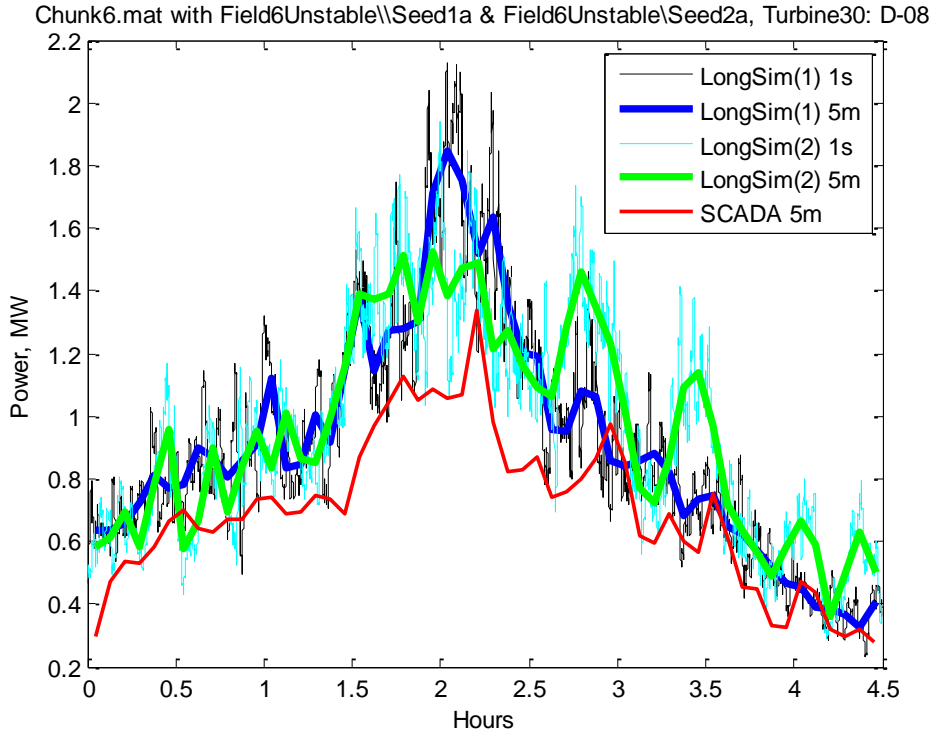


Figure 23: Power at the reference turbine (two seeds in LongSim)

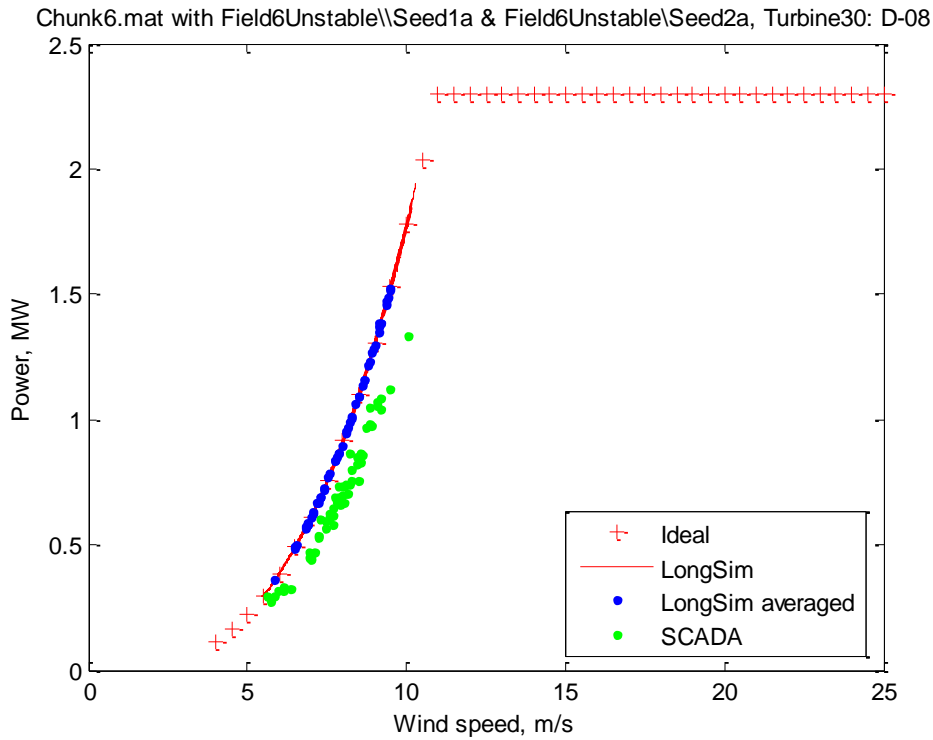


Figure 24: Power curve for the reference turbine

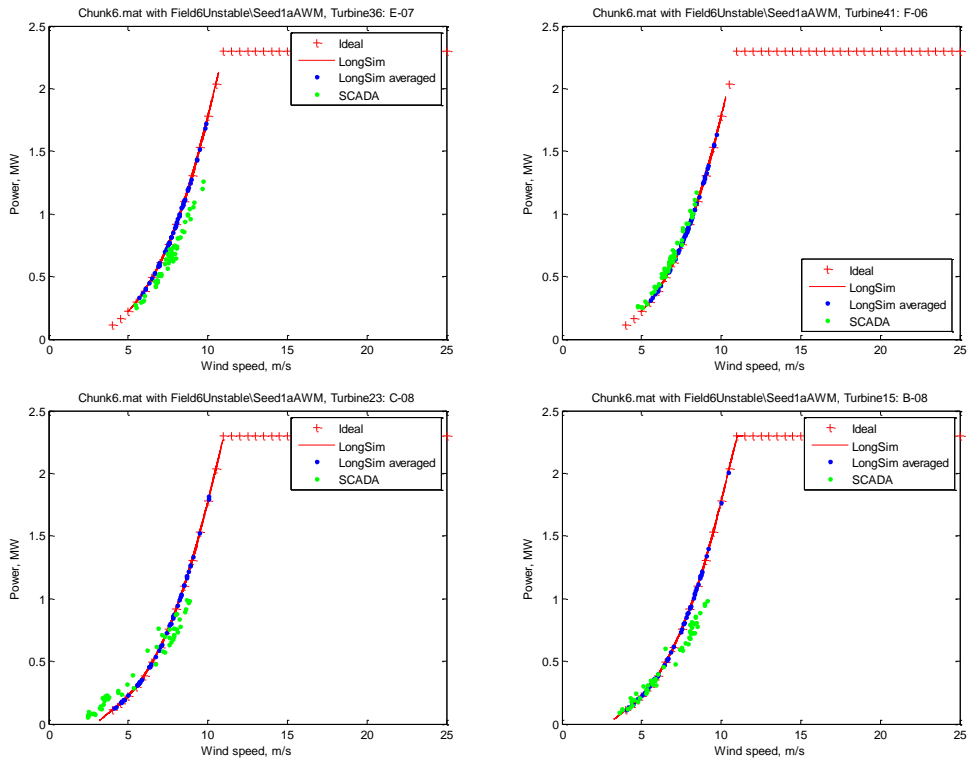


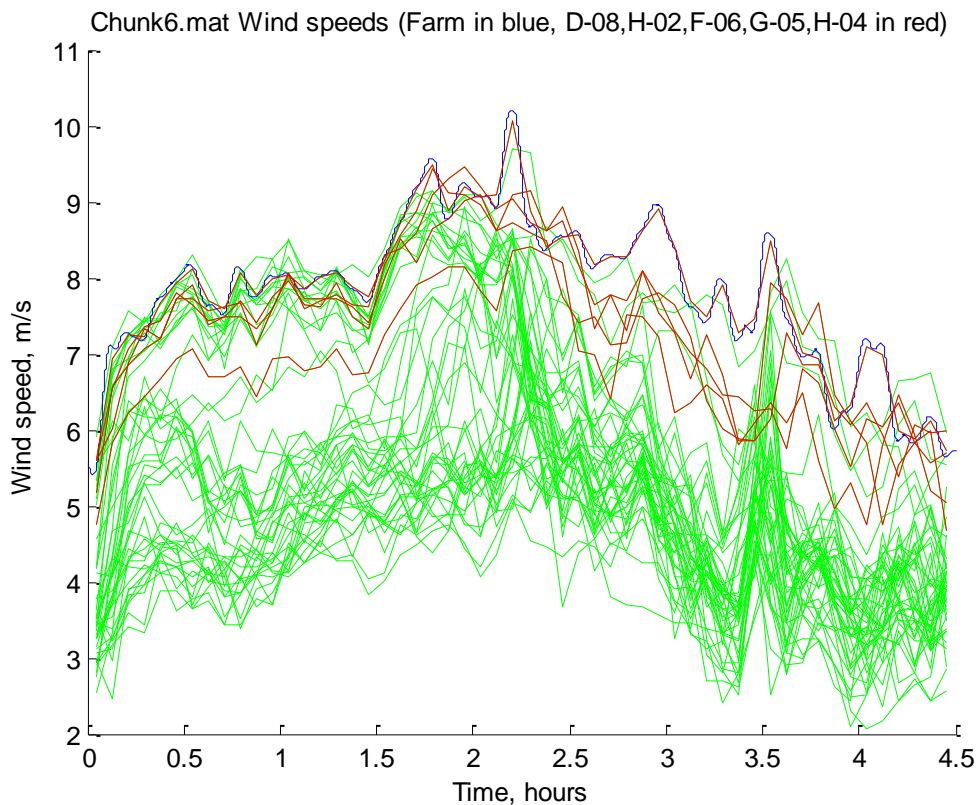
Figure 25: Power curve for the reference turbine

Figure 25 shows similar power curve plots for some of the adjacent turbines. These show a range of characteristics, all of which are seen also in some other turbines. Some, like F-06, appear to

follow the theoretical power curve very well; some like E-07 and B-08, appear to underperform like D-08, but not in very low winds; and some, like C-08, even seem to be over-performing in the very low winds, but under-performing in higher winds.

If these discrepancies are caused by inaccurate SCADA wind speed signals, this would affect the simulations because the wrong wind speeds are used to generate the wind fields used in the simulations. If the discrepancies are caused by the turbines not following the expected power curve characteristics, then the thrust coefficients may not be modelled correctly, and the wakes would then be modelled wrongly in the simulations.

To examine the measured wind speeds further, *Figure 26* shows the SCADA measured wind speeds at all the turbines during this period. The red lines are for the turbines in the west of the farm which remain unwaked during the simulation. Here we see a systematic disagreement about the wind speed, with the lowest line, which is for turbine F-06, consistently recording a wind speed more than 1 m/s below the reference turbine D-08 which has been used to represent the farm wind speed. Although wind speed differences between these turbines could conceivably be due to site inhomogeneity, this appears unlikely, especially in the case of F-06, and inaccurate measurements are almost certainly the cause. Clearly if F-06 had been used as the reference, the wind speeds throughout the farm would have been significantly lower in the simulation.



*Figure 26: SCADA wind speed time histories, with unwaked turbines highlighted*

Another thing to check is the yaw control performance of the turbines, since the yaw control logic is not known, and so some standard assumptions were made, as explained in Section 3.1.1. *Figure 27* shows the modelled yaw performance of two turbines, the reference turbine D-08 and A-01 which is far downstream. In both cases (also true for all the turbines), the yaw tracking is

good, with misalignments kept well below 10 degrees most of the time, and the frequency of yaw manoeuvres kept sufficiently small. The SCADA data does not include the wind vane signal, so it is not possible to see the yaw misalignments in the measured data, so it is not easy to judge whether yaw control might account for any power discrepancies, but it seems unlikely, given the nature of the discrepancies illustrated in *Figure 25*. The raw SCADA data could be examined to see whether the frequency of yaw manoeuvres is about right, but this has not been attempted.

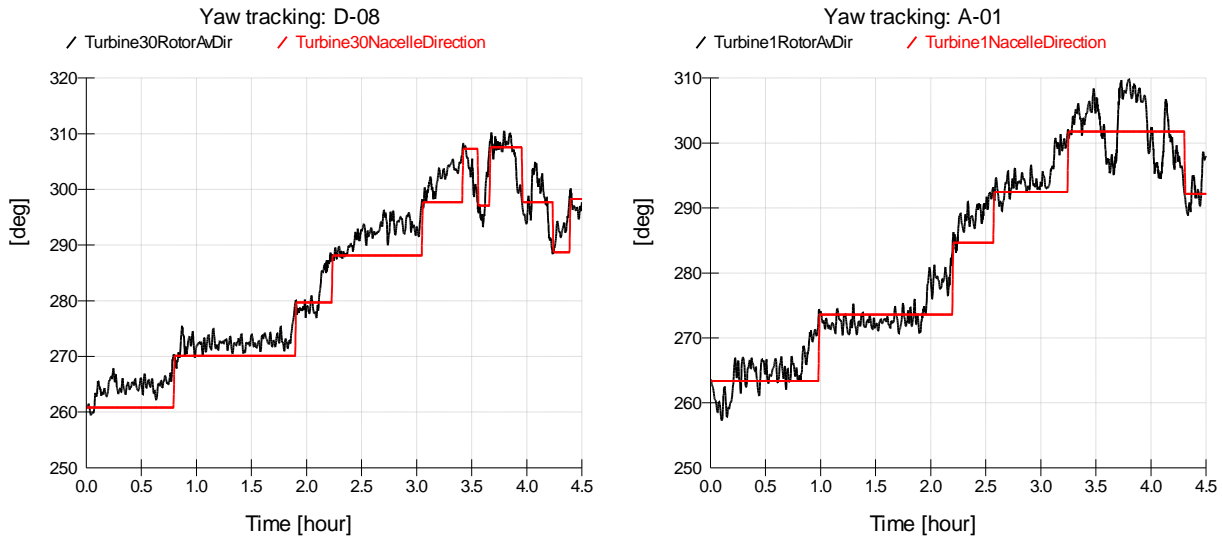


*Figure 27: Yaw tracking performance*

A further uncertainty is that the SCADA dataset does not provide any measured thrust or other signals from which the thrust coefficients of the turbines could be confirmed. Any mis-match in thrust coefficients would clearly affect the wakes.

We will now look at some of the wake-affected turbines, as well the un-wakes ones. With winds from westerly directions, the most wake-affected turbines are mostly in the area around A-01. Turbines in the middle of the farm are quite heavily wake-affected, but D-04, C-04 and C-05 less so because of the ‘hole’ where two turbines are missing from row 5.

A useful way to look at wake effects is to consider the power ratio between a given turbine and the un-waked reference turbine, as a function of wind direction. This avoids some of the problems caused by uncertainty in overall wind speed levels. For un-waked turbines, the ratio should be close to 1, as confirmed by the examples of E-07, F-06 and H-04 in *Figure 28*. Particularly for the larger wind directions, the scatter and the divergence between *LongSim* and SCADA results appear to increase with distance away from the reference turbine D-08. This might just be because the simulation is not long enough to average out the effect of low-frequency coherence in wind direction.

Power ratios for slightly waked turbines behind the ‘hole’ in row 5 are plotted in *Figure 29*. Now we see ratios much less than 1. The directional variation in the SCADA data is reproduced well by the *LongSim* results. The actual power ratios are well predicted in the middle part of the direction range, but are generally higher in the *LongSim* results towards the smaller and larger directions, perhaps because the inter-turbine spacing in the along-wind direction is then smaller; in fact at 300° the spacing is just 3.3 diameters, and the wake model may not fit as well for such an untypically small spacing,

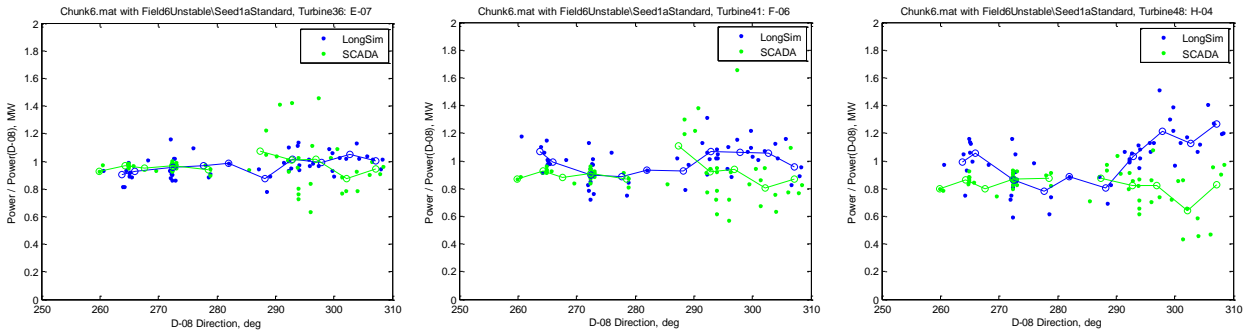


Figure 28: Power ratios for unwaked turbines, and 5° direction bin averages (E-07, F-06, H-04)

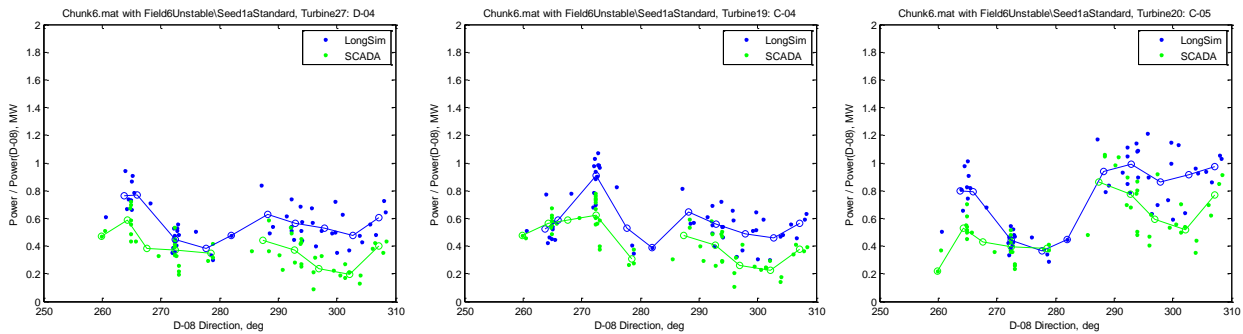


Figure 29: Power ratios for turbines D-04, C-04 and C-05, and 5° direction bin averages

Finally, power ratios for a few more heavily waked turbines are shown in Figure 30. Again, the general patterns are well reproduced by LongSim, but there is a tendency for some over-prediction of the power for the directions in which the turbines are most closely spaced.

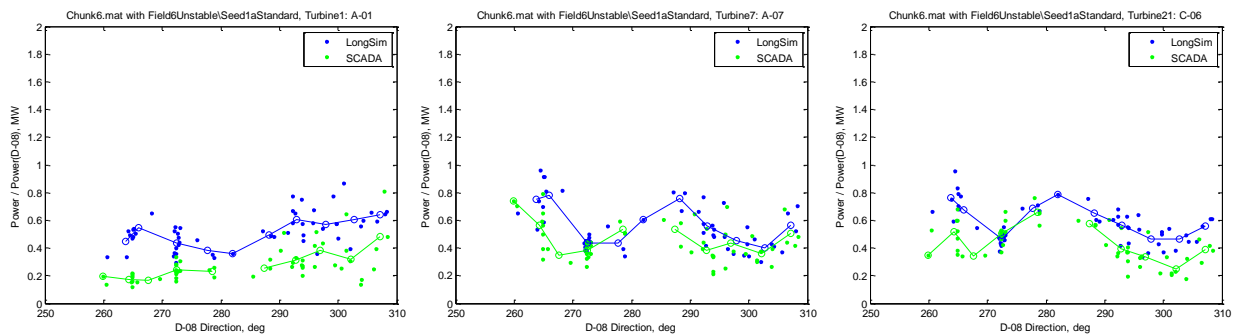


Figure 30: Power ratios for turbines A-01, A-07 and C-06, and 5° direction bin averages

Because of this over-prediction, the total wind farm power is also significantly over-predicted, as shown in Figure 31. This may be expected from Figure 26, which indicates that the wind speed measured at the reference turbine, which is used to drive the simulation, may be higher than it should be.

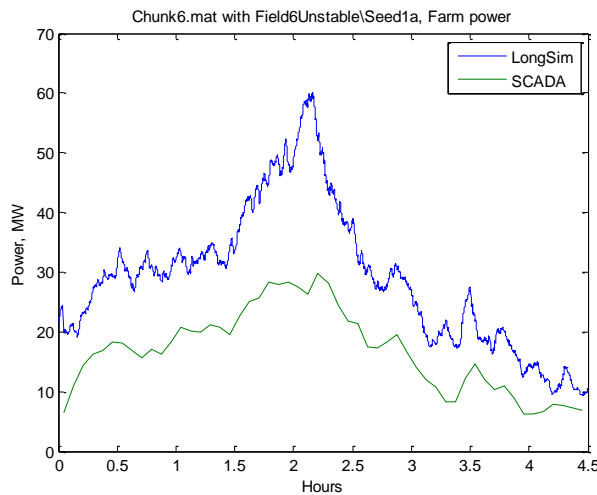


Figure 31: Total wind farm power

Further simulations were therefore done, to try to obtain better agreement with the SCADA data. Figure 32 shows the total wind farm power in red, compared to the result from two further simulations. Firstly, in green, an attempt was made to tackle the important uncertainty about the reference wind speed, by making the assumptions that (a) the D-08 measured wind speed is incorrect, (b) the measured D-08 power is correct, and (c) the theoretical power curve from the *Bladed* model is representative of the turbine. Then the D-08 power signal was used to estimate the wind speed using linear interpolation from the theoretical power curve. This estimated wind speed was then used to generate the wind field for the simulation. This gives the green line in Figure 32, which is significantly closer to the SCADA result. Then by switching to the near-neutral wake model (Obukhov length 2500m), a further small improvement is obtained. As is clear from Section 4, the stability conditions during the measurement period are not actually known, so this assumption is not unreasonable. Of course, if a stability signal were available from the SCADA data, *LongSim* could be made to change the stability dynamically during the simulation.

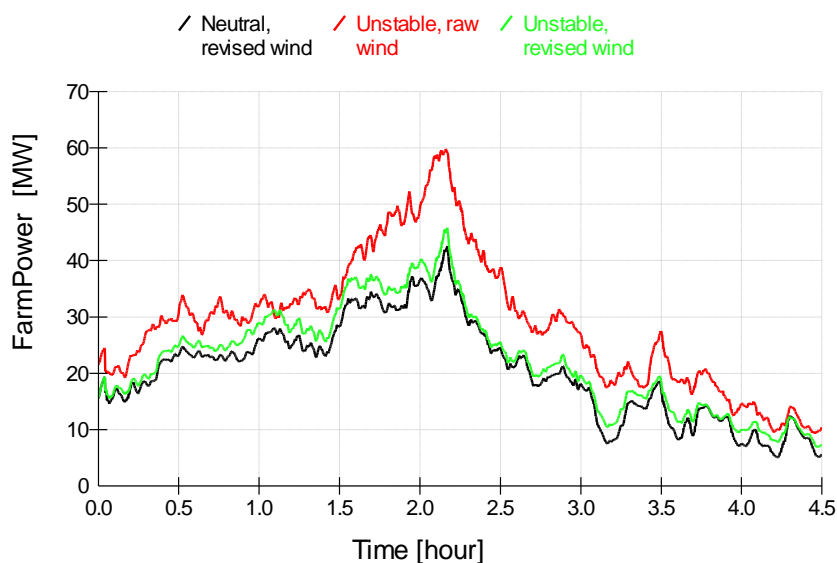


Figure 32: Total wind farm power with different assumptions

## 5.4 FURTHER SIMULATION RESULTS

This section presents similar results taken from a longer simulation (nearly 10 hours) using a wind field based on a different period of the SCADA data, here called ‘Period 2’.

Given the results of *Figure 32*, the reference wind speed signal was derived by transforming the measured power of turbine D-08 through the theoretical power curve, and the near-neutral wake model was selected. As this is different period, the atmospheric stability might be different, but no stability measurements are available. At least both are overnight periods: 18:35 to 04:20 for Period 2, compared to 22:25 to 02:50 for Period 6.

The wind conditions for these simulations are shown in *Figure 33*. The reference wind speed is reduced by about 1 m/s by using the D-08 power. Raw wind speed and direction for all the turbines are plotted in *Figure 34*. This time the reference direction seems to be rather below the average, with the same large spread between turbines as before, but in the absence of more information about the calibrations, no attempt has been made to correct for a wind direction offset at turbine D-08.

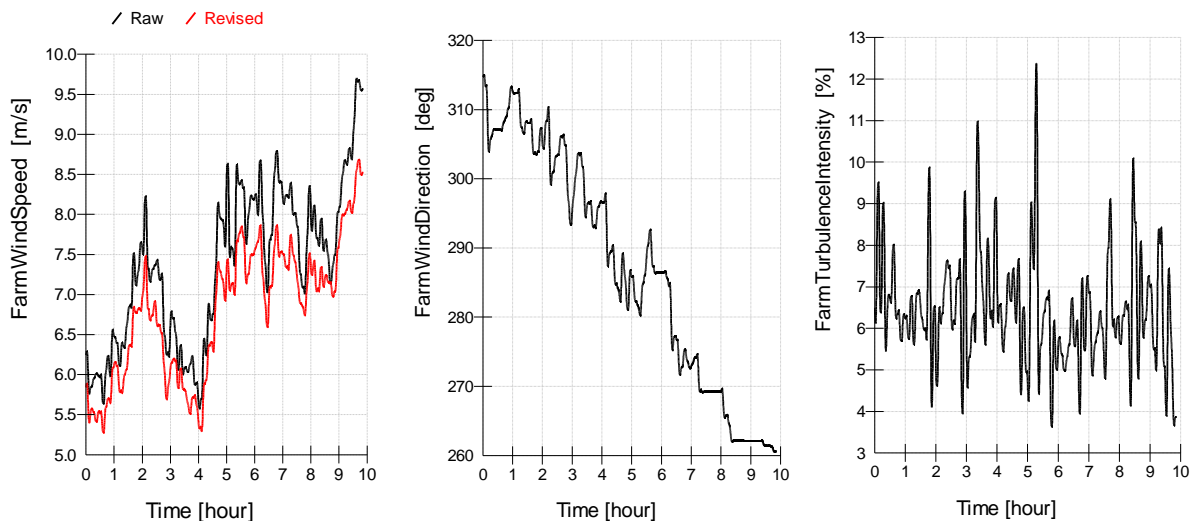


Figure 33: Wind conditions for ‘Period 2’

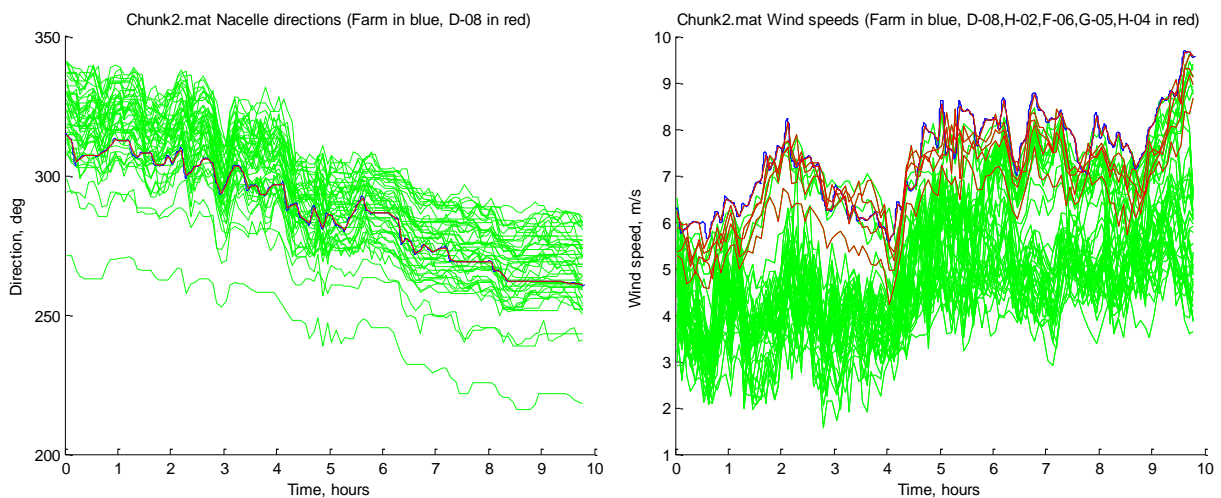
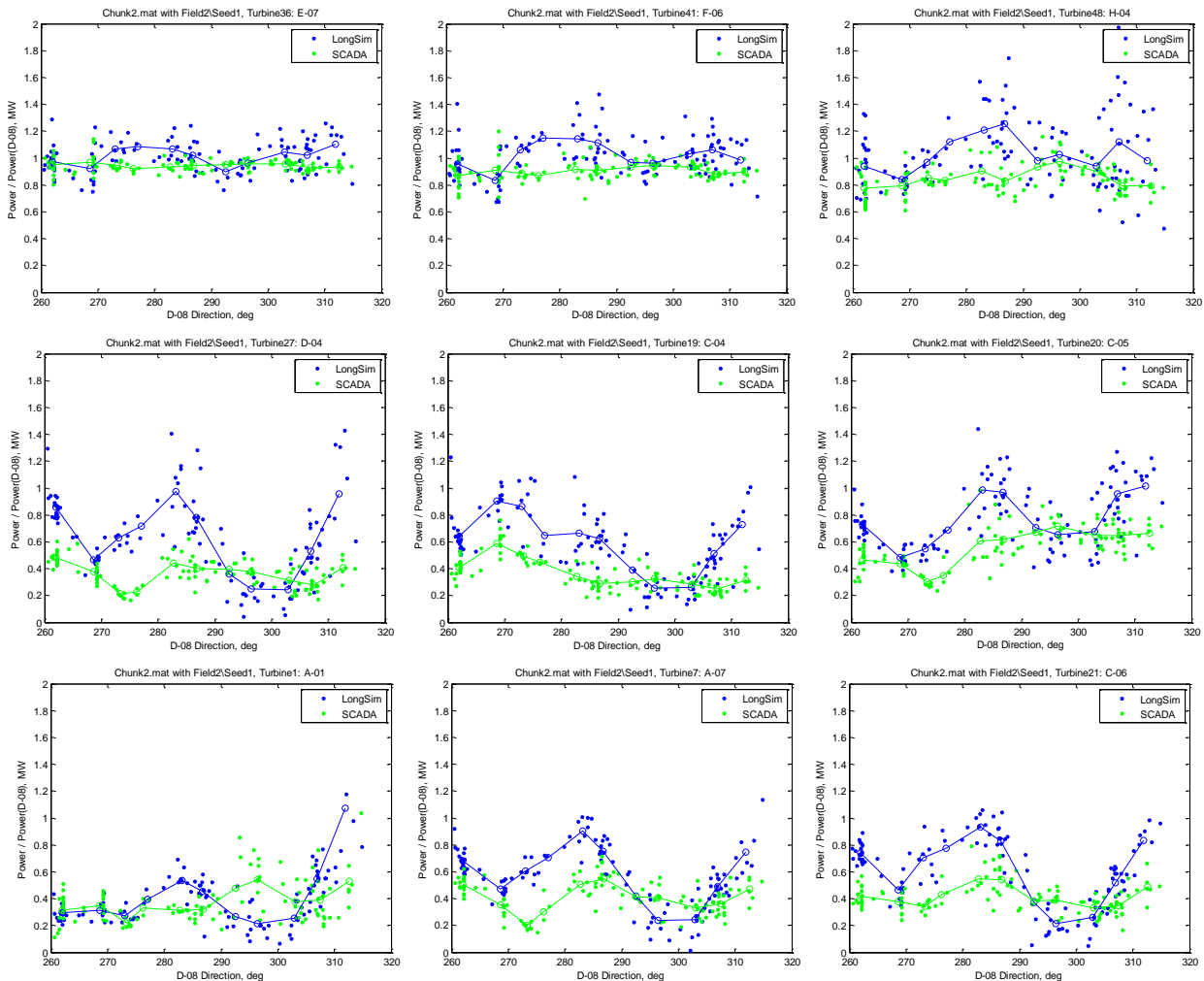


Figure 34: Raw SCADA wind speed and direction signals

Power ratios are plotted for the same turbines as before, in *Figure 35*. This time, the agreement seems best around 300°. The wind speeds at unawaked turbines now appear to be higher than the reference for many directions, so clearly the wind speed measurement issue is not perfectly resolved. The prediction of the overall wind farm power in *Figure 36* is much improved, but also still indicates that the wind speed is sometimes too high.



*Figure 35: Power ratios for the following turbines:  
 Top: unawaked turbines E-07, F-06, H-04  
 Middle: turbines D-04, C-04 and C-05  
 Bottom: turbines A-01, A-07 and C-06*

For the wake model, it is appropriate to use the wake meandering correction described in Section 2.8.5, because the wake modelling has been based on time-averaged data whereas the simulation requires an instantaneous wake model. However, this correction depends on the standard deviation of wind direction, and since the wind direction is measured only by nacelle position without wind vane information, the measured standard deviation is very small and rather meaningless. Thus, the meandering correction made no discernible difference in this case. However, a further run was done using the meandering correction, this time using a wind field generated with *LongSim*'s standard assumption about wind direction variability instead of the

measured direction standard deviation from SCADA. This again made a small difference to the results, but still barely discernible in the results plotted here. In *Figure 36*, the blue line uses the SCADA data while the green line uses the standard assumption.

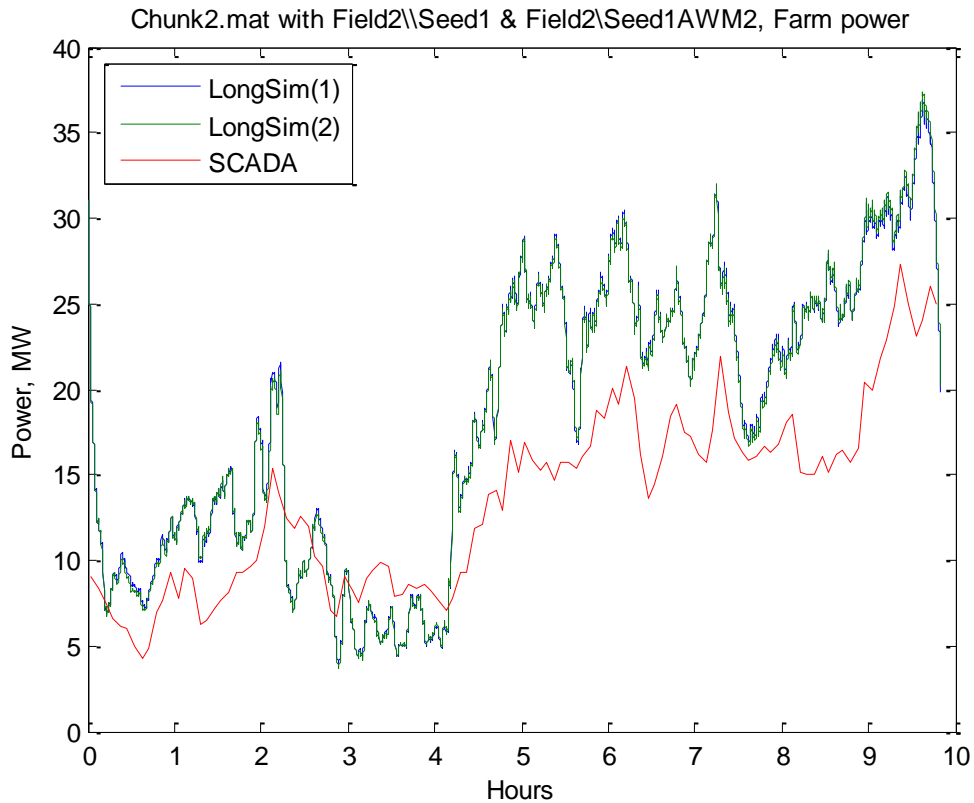


*Figure 36: Total wind farm power, with different assumptions about direction variability*

The actual power time histories are shown in *Figure 37* for the same set of nine turbines, comparing *LongSim* results against SCADA. Agreement is reasonable considering the uncertainties in the SCADA data already mentioned. Two different random number seeds are shown for the *LongSim* results. The differences between different seeds are of similar order to the differences between the simulations and the SCADA data, although for some of the more wake-affected turbines there are indications that the wake effects are sometimes generally more pronounced in the SCADA data, but not consistently so.

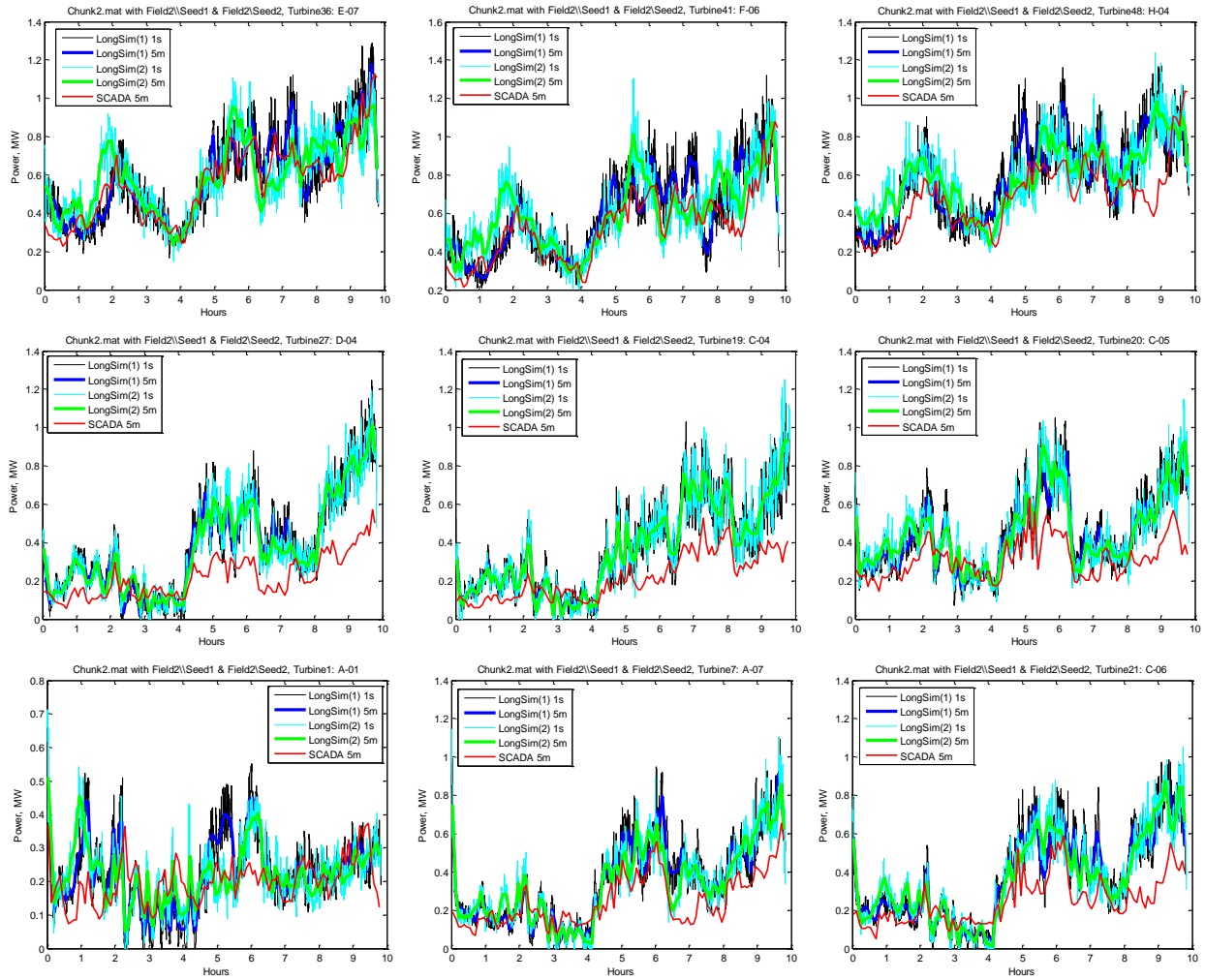


Figure 37: Power time histories for the following turbines:  
 Top: unawaked turbines E-07, F-06, H-04  
 Middle: turbines D-04, C-04 and C-05  
 Bottom: turbines A-01, A-07 and C-06

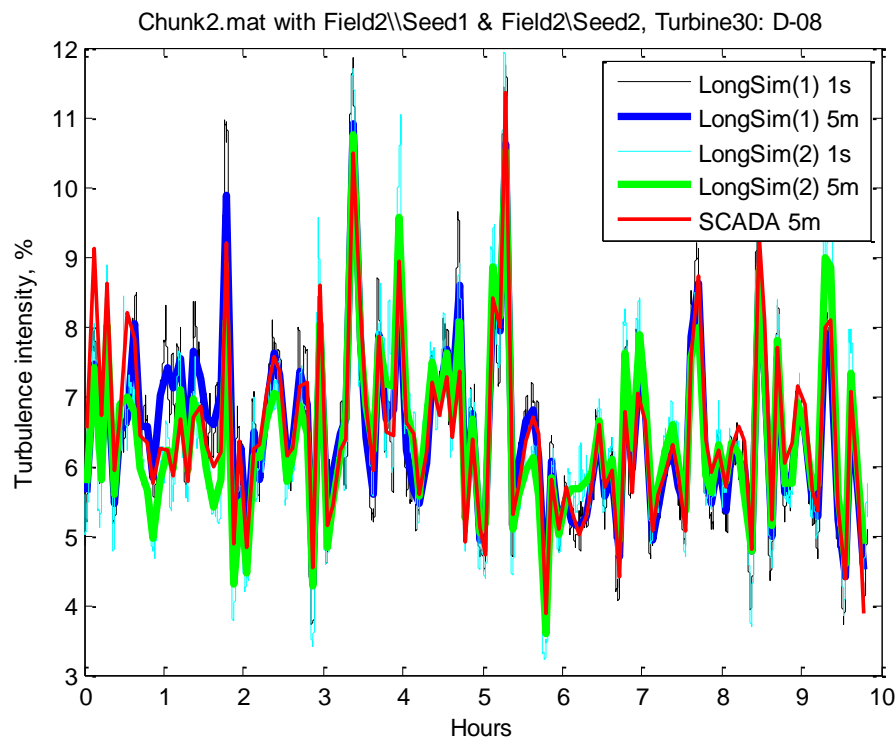
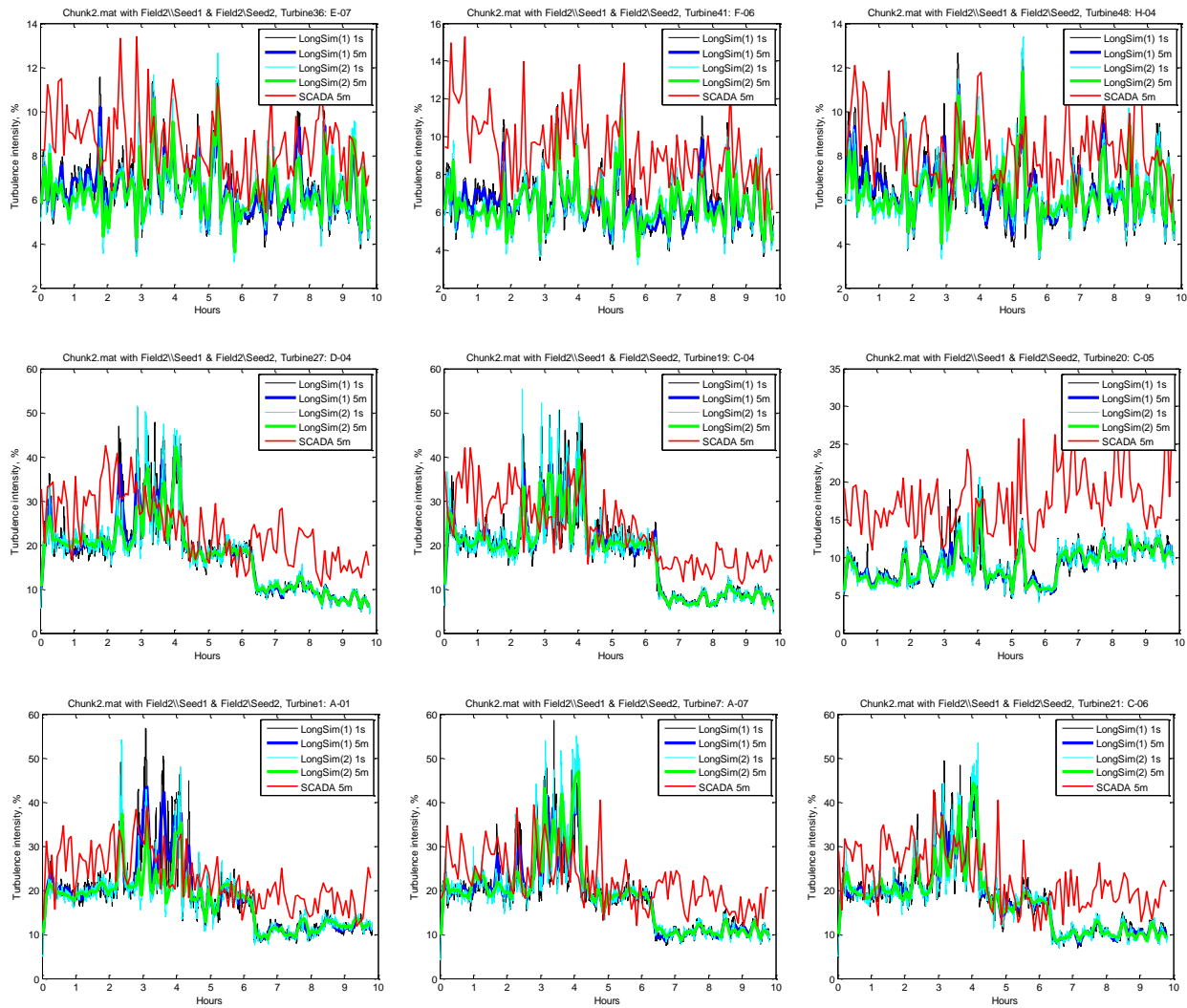


Figure 38: Turbulence intensity at the reference turbine

It is also interesting to examine the turbulence intensity, since this has a significant effect on the wake dissipation. It is also important when turbine loading is considered. Firstly, *Figure 38* confirms that the turbulence intensity in the simulation successfully follows the SCADA data for the reference turbine. Then the turbulence intensities for the same nine turbines as before (with the same two seeds) are plotted against the SCADA data in *Figure 39*. The first thing to notice is that for the other unwaked turbines, the turbulence intensity in the SCADA data is higher than it is for the reference turbine. This is a further indication of inaccuracy in the SCADA data. It may simply be because the reference turbine is recording a higher wind speed than the other unwaked turbines, as already shown, so if the standard deviation is recorded correctly, then the turbulence intensity will be lower than at the other turbines. However, if the SCADA calculates the wind speed standard deviation directly from the wind speed, then both signals would be expected to be affected in the same way, so the turbulence intensity would not change as a result. These results indicate that if a different reference turbine had been selected, not only would the wind speeds be lower in the simulation, but the turbulence intensities would be higher, resulting faster wake spreading. Therefore, this is another uncertainty in the SCADA data which affects the comparisons.

For the waked turbines in *Figure 39*, the turbulence intensity is much higher, and this increase in turbulence due to wake effects actually agrees fairly well with the SCADA data, at least for the central part of the simulation. The simulated turbulence intensity seems too low at the start and end, but this is also where the simulated power (and hence wind speed) is higher, which probably means that the standard deviation in the wakes is actually quite well predicted. The exception is Turbine C-05, where the SCADA turbulence intensity is a lot higher than predicted. Since such a large discrepancy is not present in the power for this turbine, this suggests a significant inaccuracy in the SCADA data for wind speed and/or standard deviation for this turbine.



**Figure 39: Turbulence intensities for the following turbines:**  
 Top: unawaked turbines E-07, F-06, H-04  
 Middle: turbines D-04, C-04 and C-05  
 Bottom: turbines A-01, A-07 and C-06

Finally, purely for illustration, *Figure 40* shows a contour plot of wind speeds at one instant during one of these simulations. This illustrates the spatial variation of ambient wind speed, and the turbine wakes embedded in the flow.

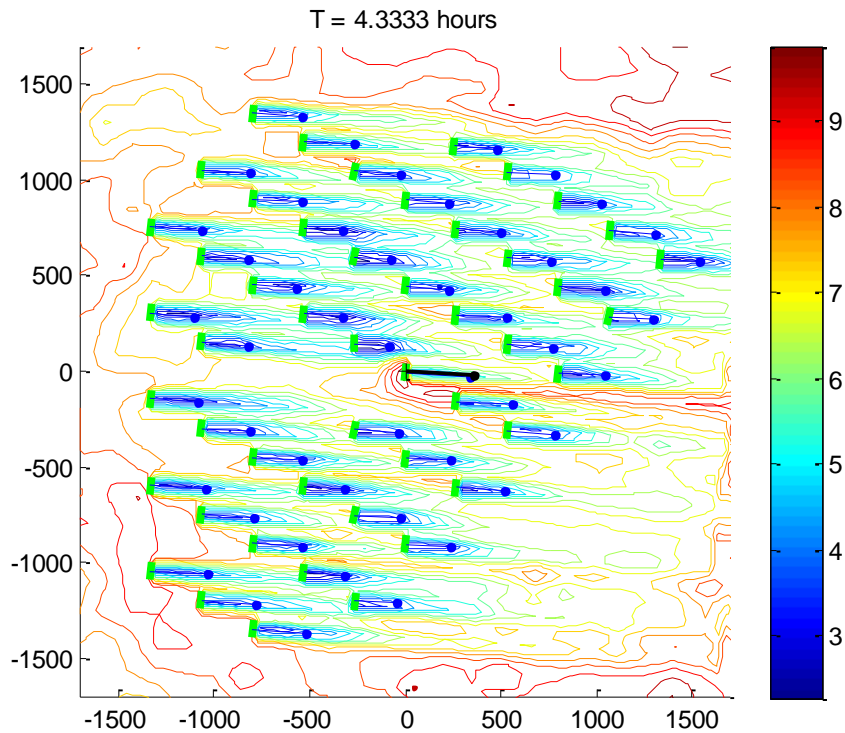


Figure 40: Example wind speed contour plot at one instant during the simulation

## 5.5 CONCLUSIONS FROM THE DYNAMIC SIMULATION RESULTS

Simulations have been run using correlated stochastic wind fields generated from 5-minute average measured wind speed, direction and standard deviation from the reference turbine D-08. Synthetic turbulence superimposed on the wind field creates variations for timescales faster than the averaging time. These fast variations will not match the unmeasured fast variations which occurred in the field at the time of the measurements, so the results have been compared on the basis of 5-minute averages. Different random number seeds can be used to create different realisations of the wind field which all match the measured data at the 5-minute level.

A number of problems were identified with the raw SCADA data which was used for the model validation. There were clearly significant errors in both the wind speed and direction data used to calculate the wind fields which drive the simulations, as well as the standard deviations. This makes it difficult to compare the simulation results directly to the SCADA results. Furthermore, some information about the turbines such as the yaw strategy and the torque and pitch control dynamics were not provided, adding further uncertainty to the comparisons.

Nevertheless, the simulation results appear to be very plausible, given these considerable uncertainties in input data. Clearly, it would be important to understand the imperfections in the SCADA data much better before drawing firmer conclusions, especially about some of the finer details of the simulation model.

Further validation may be undertaken in future when SCADA data uncertainties are better resolved, but the model nevertheless appears to be suitable for investigation of wind farm control possibilities, as illustrated in the next section.

## 6 APPLICATION TO WIND FARM CONTROL

### 6.1 INTRODUCTION

This section, which is beyond the original scope of this deliverable, has been included to show how *LongSim* can be used to optimise and test a wind farm controller for Lillgrund. The model has already been used previously for both wake steering and induction (power setpoint reduction) active wake controller designs.

Although *LongSim* is a time-domain simulation model, it can also generate the steady-solution for a given steady uniform ambient wind condition which is assumed to apply everywhere across the wind farm. The wakes are calculated, starting from the most upstream turbine, and the condition of each turbine is calculated. Wind farm control setpoints can be applied to the turbines, for example yaw offsets for wake steering or power delta set-points for induction control, and the steady-state solution recalculated. The setpoints are then adjusted iteratively to optimise a given merit function. This can include some combination of power, loads and any other relevant variables.

This section is presented only as an illustration of the application of the model, since too many unknowns remain to be able to do a proper design at this stage, including the following:

- a) Clearly, much work is needed on cleaning up and understanding the SCADA data before the validation of the model, both in terms of wake modelling and dynamic behaviour, can be completed to a more satisfactory level of detail.
- b) For wake steering, the power and thrust characteristics still need to be calculated as a function of yaw angle, to replace the assumptions detailed above. This can be done in steady state using the *Bladed* model described above.
- c) For induction control, the power and thrust characteristics still need to be calculated as a function of power reduction (delta) set-point. This can also be done in steady state using the *Bladed* model, but a dynamic model which includes the main torque and pitch control loops would be helpful, so that the rotor speed and pitch degrees of freedom are properly modelled.
- d) The actual yaw control algorithm should be used, as this makes a difference especially in the wake steering case.

Because of these points, a single illustration of wake steering control is presented, in which the simple assumptions about the yaw characteristics of the turbine are used, as detailed in Section 3.1. First, in Section 6.1.1, *LongSim* is used in a steady-state fashion to generate optimised yaw setpoints for a range of conditions, and then in Section 6.1.2 it is used to test the effect of the wake steering control by running a dynamic simulation using one of the wind fields described in Section 5.2.

A wind farm induction controller can be designed and tested in just the same way using *LongSim*. This has not been included here. However, it would be possible to do a full design of both a wake steering and an induction controller for use later in the project on the Lillgrund wind farm.

#### 6.1.1 WAKE STEERING – SETPOINT OPTIMISATION

*LongSim*'s built-in setpoint optimiser, which uses the model's steady state solution capability, was run to optimise the yaw offsets at each turbine for a set of wind conditions. The turbine yaw characteristics were assumed as already described. Yaw offsets were assumed to be allowed in the range  $\pm 30^\circ$ , and the merit function to be maximised was taken to be simply the total energy

production of the wind farm for each wind condition, ignoring loads. The unstable Ainslie-based model with Obukhov length  $L = -105\text{m}$  (see Section 5.3) was used for the wakes.

The optimiser automatically runs through all specified wind conditions, defined by combinations of wind speed, wind direction and turbulence intensity, and generates a multi-dimensional lookup table of optimised yaw setpoints. The wind conditions were specified as follows:

Wind speeds: 7 – 9 m/s in 1 m/s steps  
 Directions: 250° – 320° in 5° steps  
 Turbulence intensities: 6% only

These wind conditions cover the range found in the ‘Period 2’ sample of wind conditions which was used for the simulations described in Section 5. Normally, of course, the optimal setpoints would be calculated over the full range of conditions likely to be experienced.

Examples of the optimised setpoints are shown in *Figure 41* for three turbines, as a function of wind direction. In this case, the optimal setpoints do not change much with wind speed. This is not always the case, but here the three wind speeds are all below rated where the thrust coefficient should be the same in each case.

The increase in the total power output as a function of wind direction is shown in *Figure 42*. Again, the percentage increase varies little with wind speed.

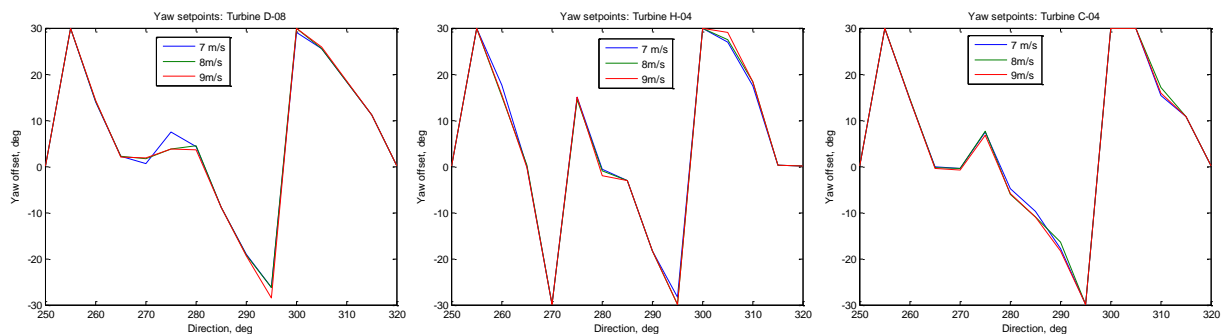


*Figure 41: Optimised yaw setpoint examples: turbines D-04, H-04 and C-04*

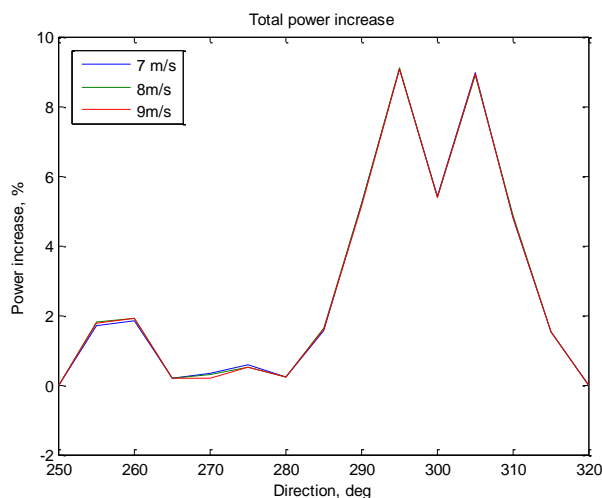


*Figure 42: Wind farm power increase predicted with wake steering in steady state*

### 6.1.2 WAKE STEERING – TESTING IN DYNAMIC SIMULATION

The steady-state optimisations in the last section indicate that there is clear potential for increased energy production by applying wake steering control at Lillgrund wind farm. However, this does not mean that these gains can be achieved in real life, because of both spatial and temporal variations in wind conditions, wake meandering, imperfect tracking of wind conditions from measurements, imperfect application of setpoints by turbine controllers, etc. Therefore, the next step is to construct a wind farm control algorithm which tries to implement the yaw offsets in a way which follows changing wind conditions, and to test this algorithm in a realistic dynamic time-domain simulation, which is what *LongSim* is designed to do.

An algorithm which can work in real life would need to perform the following steps, as a minimum:

- Estimate the current wind condition
- Use this to interpolate setpoints from the steady-state lookup table
- Send these setpoints to the turbines, which have to implement them through the turbine controller.

For the purposes of this illustrative work, a very simple algorithm has been implemented, and tested using a simulation in *LongSim* using the same ‘Period 2’ wind field as in Section 5.4 above. Then the performance of the wind farm with and without the wind farm control can be compared in identical conditions. The near-neutral wake model (Obukhov length 2500m) has been used as in those simulations, even though the setpoint optimisation used the unstable wake model. This introduces some realistic real-world uncertainty, since the stability conditions will not be known precisely, helping to give some confidence about the robustness of the control scheme to uncertain conditions.

The algorithm has been implemented as follows. First, to estimate the current wind condition, the algorithm uses an approximate wind direction to decide which turbines are currently unawaked. It then calculates the average wind speed, direction and turbulence intensity across all those unawaked turbines, and assumes that those ambient conditions prevail across the wind farm. These conditions are low-pass filtered with a 150s time constant (roughly representative of the advection time from the front row to the middle of the wind farm). It then uses these filtered conditions for interpolation of the setpoint lookup table, and calculates a yaw offset for each turbine. The simplest thing to do then is to send the yaw offsets to each of the turbines, where the standard yaw controller would use the offset just like a wind vane calibration offset. However, this means that the response of each turbine is then dictated by its own yaw control logic, with averaging time, dead-band hysteresis, etc. If a change to the turbine yaw control algorithm is permissible, however, it may be better for the wind farm controller to dictate the response more closely. Here, each yaw offset has been added to the estimated wind farm wind direction to give a demanded yaw position for each turbine. The demanded yaw position is updated every 30 seconds. Each turbine starts to yaw whenever the demanded yaw position is more than 4° different from the measured nacelle position, and stops when the two are equal. The parameters mentioned above which control this logic are first guesses, and ideally the simulations should be repeated to find the best values, but this has not been done here.

With that setup, the relevant simulation from Section 5.4 has been repeated with the wind farm control switched on. *Figure 43* shows the total wind farm power with and without the wake steering control. This shows a clear increase in power especially in the first half of the simulation.

The red line shows the increase predicted by interpolating from the quasi-static power increase (*Figure 42*) using the wind farm ambient wind conditions (derived from the unwaked turbines as described above). Particularly in low winds, the achieved increase in power production is actually significantly greater than it would be according to the quasi-static calculation. This surprising result must be due to dynamic effects in the simulation, such as wake meandering and advection, and the non-uniform ambient wind field, and perhaps variations in turbulence intensity. Also, the largest increase is obtained in wind speeds below 7 m/s, while the setpoint optimisation was only done for 7 – 9 m/s.

For this simulation, the mean power increase is 6.5%, compared to 2.6% according to the quasi-static calculation.

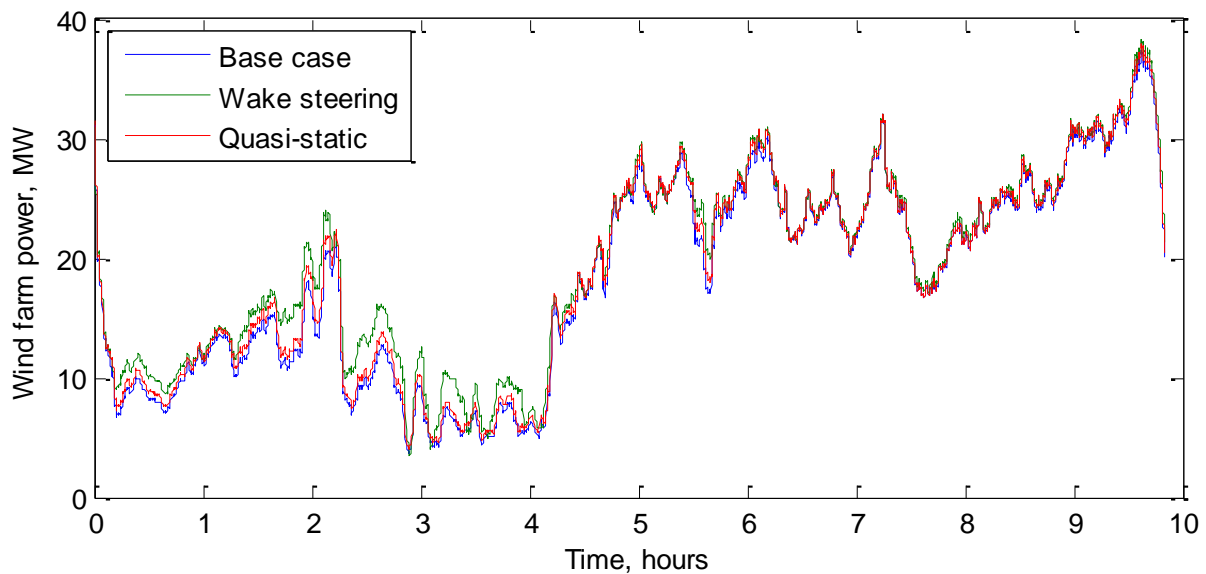


*Figure 43: Simulated wind farm power with and without wind farm control*

To illustrate the yaw behaviour of an individual turbine, *Figure 44* shows how one particular turbine, D-08, responds during the simulation. The demanded yaw offset was converted to a nacelle position demand (upper graph) which the actual nacelle position follows well through the yaw control logic defined above. The rotor-average wind direction at the turbine is also shown, demonstrating how the wake steering control is introducing a yaw offset. The lower graph shows how the actual yaw error follows the demanded yaw offset.

*LongSim* records simulated supervisory control activity during the simulations, so it is possible to keep track of, for example, the yaw control actuator duty. For the simulations presented in this section, the yaw control resulted in the following statistics:

	No. of yaw events	Total yaw travel [deg]
<b>Base case</b>	1088	10268
<b>Wake steering</b>	3935	20435

In this case, the wake steering resulted in a considerable increase in yaw actuator duty. However, a subsequent part of the wind farm controller design process is to modify the various parameters such as the controller update frequency, averaging time, hysteresis dead-band etc. to achieve

the best trade-off between energy production and actuator duty. *LongSim* is ideally suited to this task. Since the wind fields are based on actual site data, they embody site-specific low-frequency variations, which are important in determining the amount of yaw activity.

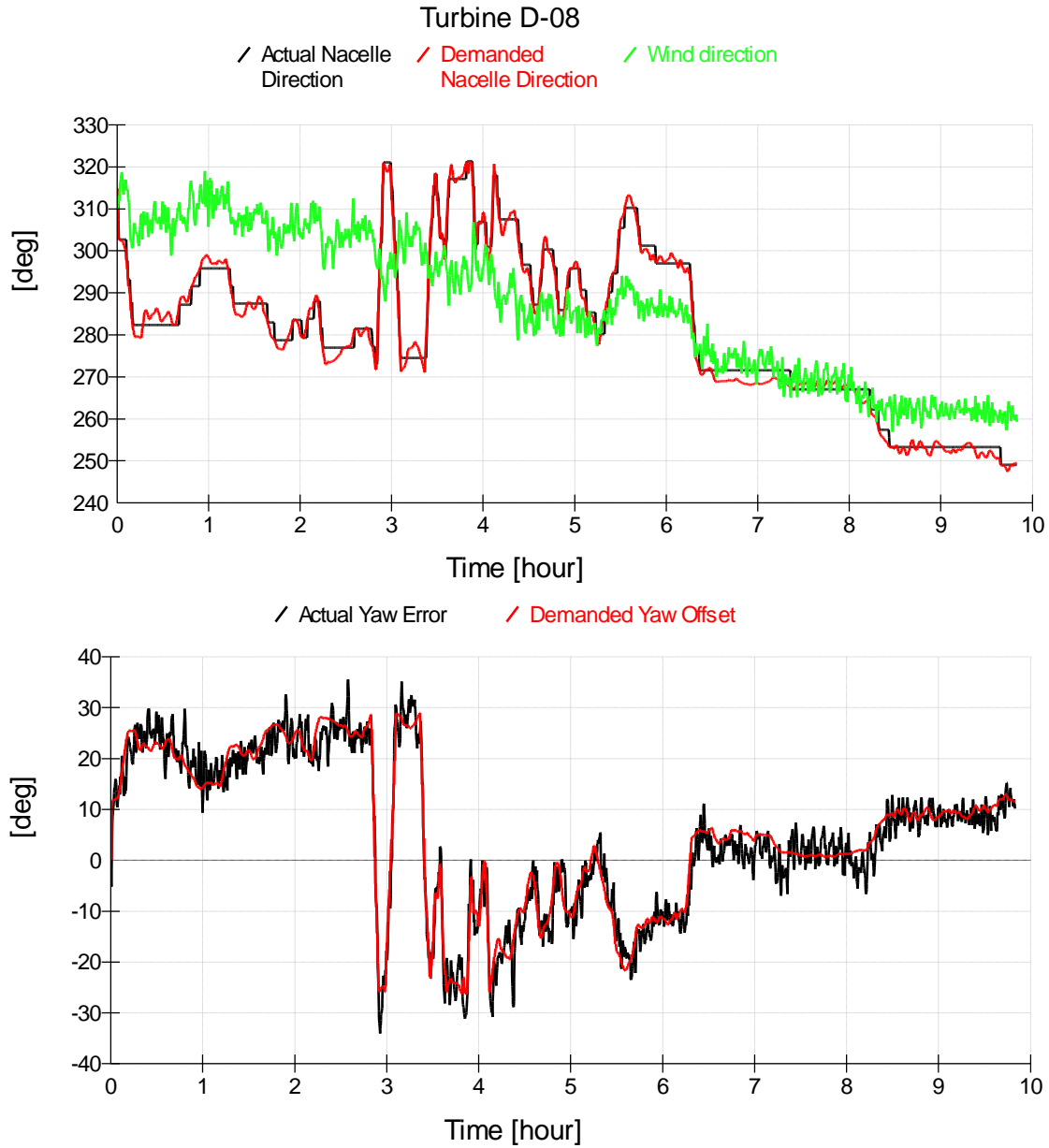


Figure 44: Turbine yaw control example: Turbine D-08

## 7 CONCLUSIONS

This report draws three main conclusions relating to the *LongSim* model, relating to wake modelling, dynamic simulation of wind farms, and the application to wind farm control.

### 7.1 WAKE MODELLING

The mean power signals provided within the 5-minutes averaged SCADA dataset were used to compare different wake models which are available in *Longsim*. A study on the atmospheric stability conditions at the site was performed based on nonconcurrent data from the nearby Drogden lighthouse, from which a potential link between strong unstable conditions and time-of-day was found. Comparisons were performed both for narrow wind direction bins ( $300^{\circ}\pm 2.5^{\circ}$ ) and larger wind direction bins ( $300^{\circ}\pm 15^{\circ}$ ), and with different filtering strategies. A modified-Ainslie wake model, which was tuned for unstable atmospheric conditions, was found to perform better in terms of power predictions compared to the other models considered, for the simulations performed with a directional bin of  $30^{\circ}$ . This model also performed reasonably well for the predictions carried out with a narrower directional bin of  $5^{\circ}$ . The Windfarmer model, based on the assumption of neutral atmospheric conditions, is found to perform reasonably well when compared to power production filtered for narrow directional bins: it is believed that this advantage might derive from the bias toward the dominant-wake superposition assumption (used in this wake model) which might perform better than the sum-of-deficit wake superposition model used in the other wake models; however this is not demonstrated in this study.

It is noted that the small inter-turbine spacing and the uncertainties on the non-calibrated SCADA data will affect the predictions.

### 7.2 DYNAMIC SIMULATION

Starting from 5-minute averaged reference turbine wind signals from the Lillgrund SCADA dataset, *LongSim* has been used to add synthetic turbulence to generate correlated stochastic wind fields covering the whole area of the Lillgrund wind farm which are representative of wind conditions at the site. These wind fields have been used as input to dynamic simulations of the wind farm performance, including the dynamics of both the turbines and their wakes, including turbine yaw control and wake meandering. The simulation results were then compared to the SCADA data for all the turbines, as a way of validating the *LongSim* model. Simulations of up to 10 hours were carried out for illustration, although *LongSim* is designed to allow much longer simulations to be run.

A number of issues were identified with the raw SCADA data which was used for the model validation. Significant problems were identified with the wind speed and direction data used to calculate the wind fields which drive the simulations, and further uncertainty resulted from the lack of complete performance and control information relating to the turbines. This made it more difficult to achieve a precise comparison between the simulation results and the SCADA data, and to validate some of the finer points of the model. Nevertheless, the simulation results appear to be very plausible, indicating that the model is suitable and appropriate for investigation of wind farm control possibilities.

### 7.3 WIND FARM CONTROL

As an illustration of the application of *LongSim* to wind farm control, the model was used in a two-step process, to design and test a wake steering controller for Lillgrund wind farm. Firstly, the model was used in steady-state mode to optimise yaw set-points for the individual turbines to achieve maximum energy production in a range of wind conditions. Secondly, the optimised set-points were incorporated into a dynamic wind farm controller which estimates the wind conditions from available data, calculate the yaw setpoints, and send commands to the turbines to modify their yaw behaviour accordingly. The model was then used to run realistic dynamic time-domain simulations, using the stochastic wind fields described above as input, with and without the wake steering control. The simulations incorporate many real-world effects which cannot be represented in the steady-state optimisation process, and can therefore give a much more reliable indication of the benefits of wind farm control which might be expected to be achievable in practice.

The results are very promising, indicating that an improvement in power performance of a few per cent may be achievable in below-rated wind conditions. This demonstrates the usefulness of *LongSim* as a tool for wind farm control design. It can also be used in the same way for induction control, where turbine power setpoints are changed to optimise overall performance. The optimiser is also capable of including loads as well as power in the merit function used for optimisation, and the dynamic simulations keep track of supervisory control events, allowing the yaw actuator duty to be calculated, for example.

## REFERENCES

- [1] “Long-term simulations for optimising yaw control and start-stop strategies”, E Bossanyi, T Delouvié and S Lindahl, Proc. European Wind Energy Conference, Vienna, EWEA 2013.
- [2] “Dynamic wind power plant simulator for wind farm controller testing”, E Bossanyi, Proc. Wind Energy Science conference, Copenhagen, June 2017.
- [3] “Combining induction control and wake steering for wind farm energy and fatigue loads optimisation”, E. Bossanyi, Proc. Torque from Wind conference, Milan 2018, (IOP proceedings).
- [4] CL-Windcon project: <http://www.clwindcon.eu>.
- [5] “Wind energy handbook”, Burton *et al*, Second edition, John Wiley & Sons, 2011.
- [6] “Generic grid frequency response capability for wind power plant”, E A Bossanyi, Proc. European Wind Energy Association Conference, Paris, November 2015.
- [7] “Three dimensional wind simulation”, P S Veers, SAND88 - 0152, Sandia National Laboratories, March 1988.
- [8] IEC 1400-1, Wind turbine generator systems - Part 1: Safety requirements, Third edition, 2004.
- [9] “Spectral structure of mesoscale winds over the water”, X G Larsen *et al*, Q. J. R. Meteorol. Soc. 139: 685–700, April 2013 A
- [10] “Atmospheric Turbulence. Models and Methods for Engineering Applications”, H A Panofsky & J A Dutton, John Wiley & Sons, 1984.
- [11] “On longitudinal spectral coherence”, L Kristensen, Boundary Layer Meteorology 16 (1979) 145-153.

- [12] “Detection of Wind Evolution and Lidar Trajectory Optimization for Lidar-Assisted Wind Turbine Control”, D Schlipf et al, *Meteorologische Zeitschrift* Vol. 24 No. 6 (2015), p. 565 – 579.
- [13] “Calculating the flowfield in the wake of wind turbines”, J F Ainslie, *Journal of Wind Engineering and Industrial Aerodynamics* **27**, 1988.
- [14] “WindFarmer Theory Manual v5.3”, DNV GL (2014).
- [15] “Turbulence in Wind Turbine Wakes”, D C Quarton & J F Ainslie, *Wind Engineering*, Vol. 14 No. 1, 1990.
- [16] “A wind tunnel investigation of the wake structure within small wind turbine farms”, U Hassan, ETSU WN 5113, 1993.
- [17] “Wake meandering – a pragmatic approach”, G Larsen et al, *Wind Energy* **11** pp377-395, 2008.
- [18] “Wake dynamics in offshore wind farms”, M de Mare, DTU Wind Energy PhD-0048 (EN), April 2015.
- [19] “Application of a LES technique to characterize the wake deflection of a wind turbine in yaw,” A. Jiménez, A. Crespo, and E. Migoya, *Wind Energy*, 13(6):559–572, 2010.
- [20] “Data-driven wind plant control”, P M O Gebraad, PhD Thesis, T U Delft, 2014.
- [21] “A new analytical model for wind-turbine wakes”, Majid Bastankhah and Fernando Porté-Agel, *Renewable Energy* 70 (2014) 116-123
- [22] “A new analytical model for wind farm power prediction”, Amin Niayifar and Fernando Porté-Agel, *Journal of Physics: Conference Series* 625 (2015) 012039  
doi:10.1088/1742-6596/625/1/012039
- [23] “Experimental and theoretical study of wind turbine wakes in yawed conditions”, Majid Bastankhah and Fernando Porté-Agel, *J. Fluid Mech.* (2016), vol. 806, pp. 506-541.  
(doi:10.1017/jfm.2016.595)
- [24] “Limitations to the validity of single wake superposition in wind farm yield assessment”, K Gunn et al., *WindEurope Summit 2016, Journal of Physics: Conference Series* 749, IOP, 2016.
- [25] FLORIS “<http://github.com/wisdem/floris>”, (NREL, Python version)
- [26] FLORISSE “<https://github.com/WISDEM/FLORISSE>”, (TU Delft, Matlab version)
- [27] “Combining induction control and wake steering for wind farm energy and fatigue loads optimisation”, E. Bossanyi, *Proc. Torque from Wind conference, Milan 2018*, (IOP proceedings).
- [28] “Optimising yaw control at wind farm level”, Ervin Bossanyi, *Proc. WindEurope annual conference, Bilbao, April 2019*.
- [29] “Field test of wake steering at an offshore wind farm”, P Fleming et al, *Wind Energ. Sci.*, 2, 229–239, 2017.
- [30] Ott S, Nielsen M 2014 Developments of the offshore wind turbine wake model Fuga, DTU Wind Energy, DTU Wind Energy E; No. 0046.
- [31] R. Ruisi, E. Bossanyi, “Engineering models for turbine wake velocity deficit and wake deflection. A new proposed approach for onshore and offshore applications.”, *pending publication WindEurope 2019*.
- [32] Dyer A J 1974 “A review of flux-profile relationships”, *Boundary-Layer Meteorol* 7:363.
- [33] Högström U 1988 “Non-dimensional wind and temperature profiles in the atmospheric surface layer: a re-evaluation”, *Boundary-Layer Meteorol*, 42: 55-78.

- [34] Crespo A, Hernandez J, 1996 “Turbulence characteristics in wind-turbine wakes”, J. Wind Eng Ind Aerodyn.
- [35] Mittelmeier, N. et al., “An analysis of offshore wind farm SCADA measurements to identify key parameters influencing the magnitude of wake effects”, Wind Energ. Sci., 2, 477–490, 2017.
- [36] Göçmen T., Giebel G., “Estimation of turbulence intensity using rotor effective wind speed in Lillgrund and Horns Rev-I offshore wind farms”, Renewable Energy 99 (2016) 524532.
- [37] DNV GL 2014 WindFarmer Validation Report, Version 5.3.